HHS Public Access

Author manuscript

Dev Biol. Author manuscript; available in PMC 2024 November 01.

Published in final edited form as:

Dev Biol. 2023 November ; 503: 10–24. doi:10.1016/j.ydbio.2023.07.007.

The transcription regulator Lmo3 is required for the development of medial ganglionic eminence derived neurons in the external globus pallidus

Shiona Biswas[1,2], **C. Savio Chan**[4], **John L.R. Rubenstein**[5], **Lin Gan**[2,3,6]

[1]The Neuroscience Graduate Program, University of Rochester School of Medicine and Dentistry, Rochester, NY 14627

[2]Department of Neuroscience, University of Rochester School of Medicine and Dentistry, Rochester, NY 14627

[3]Department of Ophthalmology and the Flaum Eye Institute, University of Rochester School of Medicine and Dentistry, Rochester, NY 14627

[4]Department of Neuroscience, Feinberg School of Medicine, Northwestern University, Chicago, Illinois 60611

[5]Department of Psychiatry and Behavioral Sciences, UCSF Weill Institute for Neurosciences, University of California at San Francisco, CA 94143.

[6]Present address: Department of Neuroscience and Regenerative Medicine, Augusta University Medical College of Georgia, Augusta, GA 30912.

Abstract

The external globus pallidus (GPe) is an essential component of the basal ganglia, a group of subcortical nuclei that are involved in control of action. Changes in the firing of GPe neurons are associated with both passive and active body movements. Aberrant activity of GPe neurons has been linked to motor symptoms of a variety of movement disorders, such as Parkinson's Disease, Huntington's disease and dystonia. Recent studies have helped delineate functionally distinct subtypes of GABAergic GPe projection neurons. However, not much is known about specific molecular mechanisms underlying the development of GPe neuronal subtypes. We show that the transcriptional regulator Lmo3 is required for the development of medial ganglionic eminence derived Nkx2.1^{+} and PV^{+} GPe neurons, but not lateral ganglionic eminence derived FoxP2^{+}

[4])**CORRESPONDENCE SHOULD BE ADDRESSED TO:** Shiona Biswas (shiona@gmail.com).

[3])AUTHOR CONTRIBUTIONS:

S.B. designed the project, performed research, analyzed data and wrote the paper with input from all co-authors. C.S.C. and J.L.R.R. obtained funding, provided input on data analysis and writing the paper. L.G. obtained funding, provided input on research and data analysis and writing the paper.

[11])DECLARATION OF INTEREST:

J.L.R.R. is cofounder, stockholder, and currently on the scientific board of Neurona, a company studying the potential therapeutic use of interneuron transplantation.

neurons. As a consequence of the reduction in PV^+ neurons, *Lmo3*-null mice have a reduced GPe input to the subthalamic nucleus.

Graphical Abstract

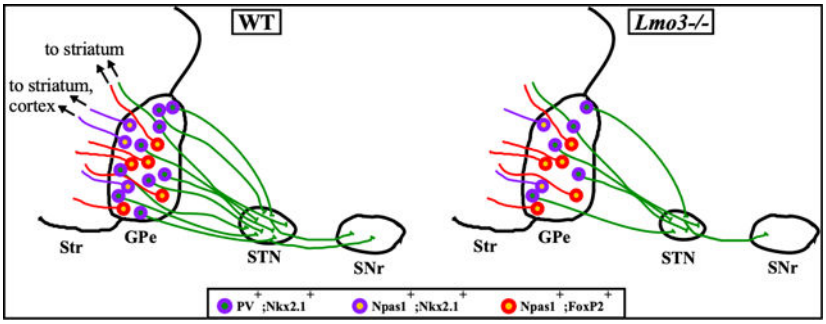

Keywords

basal ganglia; GPe; Lmo3; parvalbumin; medial ganglionic eminence

Introduction

The external globus pallidus (GPe) is a key component of the basal ganglia. By virtue of its widespread projections to all basal ganglia nuclei (Kita and Kitai, 1994; Bevan, 1998; Kita, 2007; Mallet et al., 2012; Abdi et al., 2015; Saunders et al., 2016; Glajch et al., 2016), as well as other brain regions like the cortex and thalamus (Mastro et al., 2014; Saunders et al., 2015; Abecassis et al., 2020; Lilascharoen et al., 2021; Courtney et al., 2023) it is in a unique position to influence the processing of motor information. Perturbations in the firing pattern and firing rate of GPe neurons have been linked to motor symptoms of a variety of movement disorders, such as Parkinson's Disease (Pan and Walters, 1988; Nini et al., 1995; Magnin et al., 2000; Magill et al., 2001; Starr et al., 2005; Kita, 2007; Mallet et al., 2008; Chan et al., 2011; Hegeman et al., 2016), Huntington's disease, and dystonia (Starr et al., 2005, 2008; Nambu et al., 2011; Waldvogel et al., 2014; Hegeman et al., 2016). Work from across several decades had suggested the existence of neuronal heterogeneity within the GPe, with respect to the molecular and morphological type (Iwahori and Mizuno, 1981; Hontanilla et al., 1994; Kita, 1994; Bevan, 1998; Hoover and Marshall, 1999), anatomical features (Iwahori and Mizuno, 1981; Walker et al., 1989; Kita, 1994; Kita and Kitai, 1994; Bevan, 1998; Hoover and Marshall, 1999; Cooper and Stanford, 2000) and electrophysiological characteristics (DeLong, 1971; Walker et al., 1989; Cooper and Stanford, 2000; Mallet et al., 2008). Despite this, progress was slow in understanding the cellular organization and connectivity of this structure, due to the lack of enough objective criteria that could be consistently used to define and distinguish between specific subtypes of GPe neurons (Hegeman et al., 2016).

More recently, studies have made significant progress, demonstrating that the majority of GPe projection neurons, which are GABAergic, can be divided into several different subtypes. Neurons expressing the calcium binding protein parvalbumin (PV) and those

expressing the transcription factor Nkx2.1 project primarily to the subthalamic nucleus (STN), and display faster and more regular firing *in vivo* and in *ex vivo* slice preparations, while another group of neurons that express the transcription factor FoxP2 and the opioid precursor preproenkephalin, and those expressing the transcription factor Npas1; project heavily to the dorsal striatum and typically display lower and less regular firing rates (Mallet et al., 2012; Mastro et al., 2014; Abdi et al., 2015; Dodson et al., 2015; Hernández et al., 2015; Abrahao and Lovinger, 2018; Abecassis et al., 2020; Ketzef and Silberberg, 2021). The afferent input received by different GPe neurons from other parts of the basal ganglia also differs in type and strength (Pamukcu et al., 2020; Aristieta et al., 2021; Ketzef and Silberberg, 2021; Cui et al., 2021a). As a result, they encode movement and behavior differently via distinctive changes in their firing (Dodson et al., 2015; Mallet et al., 2016) and their optogenetic manipulations alter locomotor activity in different ways (Pamukcu et al., 2020; Aristieta et al., 2021; Cui et al., 2021b). Finally, the firing of different GPe neuronal subtypes is differentially affected by dopamine loss in animal models of Parkinson's Disease (Mallet et al., 2008, 2012; Abdi et al., 2015).

It is the genetic programs initiated during brain development that ultimately generate the distinct cell types that have specialized roles in behavior (Kepecs and Fishell, 2014; Kessaris et al., 2014). In humans, haploinsufficiency or mutations of genes that are associated with neurological disorders can often be linked to brain structures whose development has been shown to be critically dependent on the homologs of the same genes, in mice (Sussel et al., 1999; Pohlenz et al., 2002; Breedveld et al., 2002; Leung and Jia, 2016). A few studies have established the spatiotemporal origins of GPe neurons (Marchand and Lajoie, 1986; Nery et al., 2002; Flandin et al., 2010; Nóbrega-Pereira et al., 2010; Dodson et al., 2015). However, specific molecular factors required for the development of GPe neuronal subtypes remain underexplored. The LIM domain containing transcription regulator *Lmo3* is strongly expressed in the developing GPe during embryogenesis (Long et al., 2009; Flandin et al., 2010, 2011), and required for the development of PV^+ cortical interneurons (Au et al., 2013), which like many GPe neurons, also originate from the medial ganglionic eminence (MGE) (Flandin et al., 2010; Silberberg et al., 2016). In this study, we address the role of Lmo3 in the development of GPe neuronal subtypes and show that it is required for the development of MGE derived $Nkx2.1^+$ and PV^+ GPe neurons, but not $FoxP2^+$ neurons. As a consequence of the reduction in PV^+ neurons, *Lmo3*-null mice have a reduced GPe input to the subthalamic nucleus.

Materials and Methods

Animals

The Lmo3-LacZ knock-in construct was generated in the laboratory of Dr Terence Rabbitts, University of Oxford. Briefly, a *LacZ* gene expressed from an EMC-IRES promoter was inserted into exon 2 of the *Lmo3* gene to interrupt the *Lmo3* coding region and generate a *Lmo3* loss-of-function allele (Tse et al., 2004). Targeted ES cells were obtained from Dr Rabbitts. Clones of these targeted ES cells were injected into C57BL/6J blastocysts to generate mouse chimeras. Heterozygous $Lmo3^{LacZ/+}$ mice were generated in 129S6 and C57BL/6J mixed

background as described before (Gan et al., 1996, 1999). The PCR primers used to identify the *Lmo3-LacZ* knock-in allele were 5'-CGAGTTCTTCAGTCAGAGTAC-3' and 5'-TCCTGCCCAGAAAGTATCCAT-3'. PCR primers used to identify the Lmo3 wildtype allele were 5'-TGCTGTCAGTTCAGCCAGAC-3' and 5'-CGAGTTCTTCAGTCAGAGTAC-3'. The $Lmo3^{LacZ/LacZ}$ homozygous mice are referred to as *Lmo3*-null or *Lmo3*−/− in the rest of the paper. $Lmo3^{LacZ/+}$ mice are referred to as *Lmo3*+/−, or heterozygous mice. *Lmo3*-null mice occasionally appeared a bit smaller in size and lighter in weight than their heterozygous and wildtype littermates but were capable of normal breeding and did not display increased mortality. We did not observe any obvious difference between the controls and mutants regarding the size of the forebrain. For the staging of embryos and adult mice, noon of the day vaginal plugs were observed was considered E0.5. For the P0 time point, pups were harvested within 24 hours of birth. Both male and female mice were used in this study. All animal procedures in this study were performed in accordance with the University Committee of Animal Resources at the University of Rochester.

Tissue preparation

For embryonic ages and P0, decapitated heads were drop fixed in 4% paraformaldehyde (PFA) for 8–48 hours at 4°C. P30 and older mice were transcardially perfused with 4% PFA followed by 30 −60 minutes postfixation at 4°C. Following postfixation, tissue was equilibrated in 30% sucrose at 4°C until it sunk to the bottom. Tissue was frozen in OCT compound (Tissue-Tek) (embryonic heads and P0 brains), or TFM medium (Electron Microscopy Sciences) (P30 brains) and stored at −80°C. Embryonic and P0 tissue was cryosectioned between 20–25 μm and collected on glass slides (Fisher) for processing while P30 and older brains cryosectioned at 40 μm and processed free-floating.

Immunohistochemistry

Sections were blocked with 10% (v/v) normal goat serum (Invitrogen) and 0.1% (v/v) Triton X-100 in PBS for 30–60 min at 4°C and were subsequently incubated in primary antibodies in 1% normal goat serum and 0.1% Triton X-100 in PBS for 24 – 48 h at 4°C. After washes in PBS, the sections were incubated with Alexa Fluor-conjugated secondary antibodies in 0.1% Triton X-100 in PBS at room temperature for 2 h. For the phosphoHistone 3 (pH3) (embryonic time points E11.5, E12.5, E13.5), caspase3 (embryonic time points E12.5, E13.5 and P0), β-gal +NeuN (P6) and Nkx2.1+FoxP2 (at P0) immunohistochemistry, antigen retrieval by heat pre-treatment (in sodium citrate buffer, pH6) was carried out prior to the blocking step. The primary antibodies and dilutions used in this study were: mouse anti-parvalbumin (1:250; Sigma P3088), mouse anti-TTF1 (Nkx2.1) (1:100; Novocastra; Leica Biosystems NCL-L-TTF-1), mouse anti-NeuN (1:500; Millipore MAB377), rabbit anti-NeuN (1:500; Millipore ABN78), goat anti-FoxP2 (1:500; Santa Cruz Biotechnology sc-21069), mouse anti-vGAT (1:1000; Synaptic Systems 131011), guinea pig anti-Bassoon (1:500; Synaptic Systems 141004), goat anti-ChAT (1:200; Millipore AB144P), rabbit anti-DARPP-32 (1:1000; Millipore AB10518), rabbit anti-phosphoHistone 3 (1:250; Santa Cruz Biotechnology), rabbit anti-Caspase3 (1:500; R&D Systems) and chicken anti-β-galactosidase (1:700; Abcam). Alexa Fluor conjugated secondary antibodies (Molecular probes) were used at a concentration of 1:1000 for all experiments except for

synaptic marker (vGAT and Bassoon) immunostaining, for which they were used at a concentration of 1:500.

in situ hybridization

in situ hybridization was performed on 20–35 μm thick sections using digoxigenin-labeled riboprobes, as described previously (Bulchand et al., 2003). The following probes were used: Lmo1, Lmo3, Lmo4, Mash1, Pax6, Isl1. Couptf1, Er81, Nkx2.1, Dlx2, Lhx6, Lhx8, Gli1 and Ptc1 (gifted by Gord Fishell).

X-Gal staining

X-Gal(5-bromo-4-chloro-3-indolyl-β-D-galactopyranoside) staining was performed on 20–30 μm thick E16.5 sections as described previously (Gan et al., 1999).

Image acquisition and data analysis

Images of *in situ* hybridization experiments were captured using brightfield. For the analysis of pH3 and ChAT immunostaining and to obtain other low magnification immunofluorescence images, Axio Imager M1 (Carl Zeiss) was used. Z stack images were obtained using a confocal microscope LSM 510 (Carl Zeiss). Z stack images were obtained with optical slices 4 μm apart using the 40x water immersion objective for analysis of P0 GPe immunostaining. Cells were counted from the entire GPe, using the ventral borders defined according to the medial edge of the anterior commissure (Fig. 2I) 3 GPe sections were analyzed for each rostrocaudal level per brain. For ~P30 (between postnatal days P30-P32) GPe immunostaining (Figs. 2, 3 and 4), Z stacks were obtained with optical slices 4 μm apart using the 20x objective. Cells were counted from the entire GPe. Ventral borders were defined according to the medial edge of the anterior commissure in rostral and middle sections and drawn at the same approximate dorsoventral level as the reticular nucleus of the thalamus for caudal sections (Fig. 2I). Between 3–4 sections were analyzed for each GPe rostrocaudal level per brain. For immunostaining with multiple markers, cells were counted in individual channels before quantifying dual labeling in merged images.

For STN area quantification at P30 (Fig. 5E), 4 different STN sections between ~1.4 and 1.8 mm lateral of Bregma were analyzed per brain. For confocal analysis of bassoon and vGAT immunostaining, Z stack images were obtained at a thickness of 0.4 μm using the 100x oil immersion objective. Density of $vGAT^+$ structures and $bassoon^+/vGAT^+$ structures was assessed using the optical dissector method (West, 1999., Fan et al., 2012). Sample sites were chosen using a grid (frame size, 10 μm x 10 μm) that was superimposed randomly on each image stack. Stereological counting was done through 4.4 μm thickness of the Z-stack (commencing at an optical section ~ 4.5 μm below the slice surface). Immunoreactive structures were counted if they appeared within the sample frame and in the reference but not the adjacent optical section. $vGAT^+$ structures > 0.5 μm^2 in their maximal cross-sectional area were first selected and then $bassoon^+$ structures that co-localized with them were subsequently counted.

Analyses were performed blind to genotype, using Image J (NIH). Statistical analyses were performed with Prism6 (GraphPad) and Microsoft Office Excel. All sample sizes (*n* values) reported represent the number of mice.

Results

Lmo3 is expressed in the progenitor zones of the developing globus pallidus

Birthdating experiments in rodents have demonstrated that GPe neurons are born between ~E10.5 and E13.5, with the PV^+ subset generated primarily from E10.5 to E12.5, while FoxP2 expressing and Npas1 expressing GPe neurons arise mainly between E11.5 and E13.5 (Marchand and Lajoie, 1986; Nóbrega-Pereira et al., 2010; Dodson et al., 2015; Hu et al., 2017). Furthermore, neuronal subtype identity in the GPe is also partly encoded by place of origin. $Nkx2.1^+$ and PV^+ neurons arise mainly from the MGE while approximately half of the $Npas1^+$ neurons are born in the MGE progenitor zone and the rest, which also express FoxP2, are born in the lateral ganglionic eminence (LGE) and/or the caudal ganglionic eminence (CGE) (Sussel et al., 1999; Flandin et al., 2010; Nóbrega-Pereira et al., 2010; Dodson et al., 2015; Silberberg et al., 2016). Fate mapping experiments have also revealed the preoptic area (PoA) as the source of a small fraction (~10%) of GPe neurons, the majority of which express PV and Nkx2.1 (Nóbrega-Pereira et al., 2010; Abecassis et al., 2020).

More recently, single-cell RNA-sequencing experiments have shown that *Lmo3* is expressed in MGE cells differentiating into GPe neurons and cortical interneurons (Su-Feher et al., 2022). Thus, we carried out an expression analysis of *Lmo3* via *in situ hybridization* at various embryonic time points and detected *Lmo3* expression from E11.5 onwards throughout the subventricular zone (SVZ) of the MGE, LGE, PoA, and the developing GPe. (Fig. 1A–D, A'–C', a'–c') *Lmo3* expression is maintained in the GPe as well as neighboring regions of the basal ganglia like the striatum, at birth (Fig. 1E) and weakly expressed at P30 (Fig. 1F, f).

Lmo3-null mutants display a selective reduction of MGE derived GPe neurons

We immunostained *Lmo3*-null mutant brains for PV and a general neuronal marker NeuN at postnatal day (P)30 (Fig. 2A–H). As PV^+ cell density varies along the mediolateral axis of the GPe (Hontanilla et al., 1994; Kita, 1994; Abecassis et al., 2020), cell counts were obtained from the entire GPe, in tissue planes at 3 different rostro-caudal levels (Fig. 2I). The number of neurons marked by NeuN was found to be decreased in the *Lmo3*-null ($rostral_{WT}$ = 815.3 ± 60.8, $rostral_{Lmo3-/-}$ = 586.2 ± 41.7, p = 0.02; $middle_{WT}$ = 687.8 ± 20.1, $middle_{Lmo3-/-}$ = 556.1 ± 12, p = 0.001; $caudal_{WT}$ = 483.4 ± 30.7, $caudal_{Lmo3-/-}$ = 378.5 ± 11.8, p = 0.02; two-tailed *t* test, n=4 mice for both genotypes; Fig. 2 J,K,L). In the *Lmo3*-null, PV^+ neurons were also reduced throughout the rostro-caudal extent of the GPe compared to the wildtype (WT) control ($rostral_{WT}$ = 372.9 ± 6.9, $rostral_{Lmo3-/-}$ = 236.5 ± 20.8, p = 0.005; $middle_{WT}$ = 301.3 ± 17, $middle_{Lmo3-/-}$ = 163.6 ± 23.7, p = 0.005; $caudal_{WT}$ = 187.8 ± 17.4; $caudal_{Lmo3-/-}$ = 84.4 ± 5.4, p = 0.001; two-tailed *t* test, n=4 mice for both genotypes). This corresponds to a PV^+ reduction in the *Lmo3*-null by 36.5 ± 5.6%, 48.5 ± 8.6% and 53.8 ± 5.3% of the values of control for rostral, middle, and

caudal levels, respectively. PV^+ and $NeuN^+$ counts in *Lmo3*+/− mice were not significantly different compared to the WT (For PV, $rostral_{Lmo3+/-}$ = 328.3 ± 21.9, $middle_{Lmo3+/-}$ = 258.5 ± 9.3, $caudal_{Lmo3+/-}$ = 195.5 ± 9.8; rostral $p = 0.17$, middle $p = 0.11$, caudal $p = 0.71$; For NeuN, $rostral_{Lmo3+/-}$ = 834.2 ± 41.3, $middle_{Lmo3+/-}$ = 711.5 ± 31.3, $caudal_{Lmo3+/-}$ = 531.5 ± 24; rostral $p = 0.82$, middle $p = 0.53$, caudal $p = 0.26$, two-tailed *t* test, n=3 *Lmo3*+/− mice; Fig. 2 J,K,L).

GPe neurons are classified based on their combinatorial expression of several molecular markers: like PV^+ neurons, all $Nkx2.1^+$ neurons originate from the MGE. While most PV^+ neurons also express Nkx2.1, a subgroup of $Nkx2.1^+$ neurons does not express PV (Nóbrega-Pereira et al., 2010; Abdi et al., 2015; Dodson et al., 2015; Abecassis et al., 2020). There can be minor differences in the functional characteristics of GPe neuronal subtypes based on the combination of molecular markers expressed. For example, $Nkx2.1^+;PV^+$ neurons have faster firing rates *in vivo* than $Nkx2.1^+;PV^-$ neurons (Abdi et al., 2015; Dodson et al., 2015). To further explore the role of Lmo3 in the development of GPe neuronal subtypes, we performed double immunostaining for Nkx2.1 and FoxP2 at P30 (Fig. 3 A–H). $Nkx2.1^+$ neurons were significantly reduced at all rostro-caudal GPe levels analyzed in the *Lmo3*-null, compared to the WT ($rostral_{WT}$ = 532 ± 56.2, $rostral_{Lmo3-/-}$ = 280.1 ± 25.1, $p = 0.006$; $middle_{WT}$ = 411.3 ± 25.6, $middle_{Lmo3-/-}$ = 215 ± 26.8, $p = 0.0018$; $caudal_{WT}$ = 312.1 ± 14.7, $caudal_{Lmo3-/-}$ = 172.7 ± 18.3, $p = 0.001$; two-tailed *t* test, n=4 for both genotypes; Fig. 3 I,J,K). $Nkx2.1^+$ neurons in the *Lmo3*-null were reduced by 46.5 ± 5%, 47.8 ± 5.1% and 50.44 ± 4.6% of the values of control for rostral, middle, and caudal levels, respectively. However, the numbers of $FoxP2^+$ neurons were unaltered in the *Lmo3*-null, compared to control ($rostral_{WT}$ = 170.6 ± 18.5, $rostral_{Lmo3-/-}$ = 195.3 ± 4.2, $p = 0.26$; $middle_{WT}$ = 158.3 ± 7.8, $middle_{Lmo3-/-}$ = 174 ± 24.4, $p = 0.57$, $caudal_{WT}$ = 142.9 ± 7.4, $caudal_{Lmo3-/-}$ = 182 ± 20.2, $p = 0.09$; two-tailed *t* test, n=4 for both genotypes; Fig. 3 I,J,K). $Nkx2.1^+$ and $FoxP2^+$ counts in *Lmo3*+/− mice were not significantly different compared to the WT (For Nkx2.1, $rostral_{Lmo3+/-}$ = 550 ± 38.3, $middle_{Lmo3+/-}$ = 489.8 ± 53.5, $caudal_{Lmo3+/-}$ = 330.1 ± 9.8; rostral $p = 0.8$, middle $p = 0.206$, caudal $p = 0.39$; For FoxP2, $rostral_{Lmo3+/-}$ = 191.9 ± 4.1, $middle_{Lmo3+/-}$ = 183.8 ± 13.4, $caudal_{Lmo3+/-}$ = 148.4 ± 6.9; rostral $p = 0.24$, middle $p = 0.18$, caudal $p = 0.62$, two-tailed *t* test, n=3 *Lmo3*+/− mice; Fig. 2 J,K,L). In agreement with previous studies (Abdi et al., 2015; Dodson et al., 2015; Abecassis et al., 2020) we did not observe any significant co-expression of Nkx2.1 and FoxP2 in the WT, which also held true for the *Lmo3*-null GPe (Fig. 3 G,H).

$Npas1^+$ GPe neurons fall into two categories: those that express FoxP2 and those that do not. $Npas1^+;Foxp2^-$ neurons express Nkx2.1 (these are $Nkx2.1^+$ neurons that do not express PV); they originate from the MGE rather than the LGE/CGE (Nóbrega-Pereira et al., 2010; Dodson et al., 2015), and can be distinguished from $Npas1^+;Foxp2^+$ neurons at postnatal ages based on the projection of the former to the cortex (with collaterals in the dorsal striatum) and thalamic reticular nucleus (Abecassis et al., 2020; Cui et al., 2021b). In addition single-cell transcriptomics analysis confirms the existence of separate $Npas1^+;Nkx2.1^+$ and $Npas1^+;Foxp2^+$ neuron clusters within the GPe (Saunders et al., 2018; Cui et al., 2021b). We obtained cell counts from ~ P30 sections double immunostained for Npas1 and Nkx2.1 (Fig. 4 A–H); excluding heterozygous mice from further analysis as no significant changes in GPe development were detected in this group. There was no

significant change in the number of Npas1$^+$ neurons in the *Lmo3*-null (rostral$_{WT}$ = 223.4 ± 6, rostral$_{Lmo3-/-}$ = 238.1 ± 16.1, p = 0.418; middle$_{WT}$ = 198.5 ± 13.2, middle$_{Lmo3-/-}$ = 216.2 ± 16.1, p = 0.237; caudal$_{WT}$ = 193.7 ± 5.4, caudal$_{Lmo3-/-}$ = 193.9 ± 10.9, p = 0.988; two-tailed t test, n=5 for both genotypes; Fig. 4 I). However, we observed a ~30% reduction in the number of Npas1$^+$;Nkx2.1$^+$ neurons (rostral$_{WT}$ = 67.7 ± 1.7, rostral$_{Lmo3-/-}$ = 46.8 ± 4.3, p = 0.011; middle$_{WT}$ = 62.8 ± 3.1, middle$_{Lmo3-/-}$ = 49.2 ± 4.1, p = 0.04; caudal$_{WT}$ = 49.9 ± 1.9, caudal$_{Lmo3-/-}$ = 34.6 ± 3.8, p = 0.012; two-tailed t test, n=5 for WT and 4 for *Lmo3*-null for rostral and caudal and n=4 for both genotypes for middle; Fig. 4 J) which was reflected in a lower percentage of Npas1$^+$ neurons co-expressing Nkx2.1$^+$ (rostral$_{WT}$ = 30.4 ± 0.88 %, rostral$_{Lmo3-/-}$ = 20.9 ± 1.4 %, p = 0.0005; middle$_{WT}$ = 32.7 ± 1.11 %, middle$_{Lmo3-/-}$ = 21.8 ± 1.4 %, p = 0.0015; caudal$_{WT}$ = 25.3 ± 1.1 %, caudal$_{Lmo3-/-}$ = 17.7 ± 1.4 %; p = 0.0044; two-tailed t test, n=5 for WT and 4 for *Lmo3*-null for rostral and caudal and n=4 for both genotypes for middle; Fig. 4 K).

We could not directly assess a reduction in the neuronal subpopulation coexpressing Nkx2.1 and PV due to technical limitations (both antibodies were raised in mouse). Given that more than 80% of GPe PV$^+$ neurons express Nkx2.1 and about two-thirds of Nkx2.1$^+$ neurons express PV (Dodson et al., 2015; Abecassis et al., 2020), it is likely that the Nkx2.1$^+$;PV$^+$ subset is significantly reduced in the mutant. In addition, our findings indicate that a small proportion of Nkx2.1$^+$ neurons that are reduced in the *Lmo3*-null belong to the Npas1$^+$;Nkx2.1$^+$ subset. The neuronal makeup of the GPe assessed using different molecular markers in the wildtype (Table 1) is consistent with values reported in prior studies from different laboratories (Nóbrega-Pereira et al., 2010; Dodson et al., 2015; Saunders et al., 2016; Abecassis et al., 2020). The table also demonstrates the difference between the percentage of total GPe neurons represented by different molecular markers in the *Lmo3*-null, compared to the WT: (PV/NeuN)$_{WT}$ = 45.9 ± 3.7, (PV/NeuN)$_{Lmo3-/-}$ = 30.4 ± 1.6, p = 0.02; (FoxP2/NeuN)$_{WT}$ = 24 ± 1, (FoxP2/NeuN)$_{Lmo3-/-}$ = 40 ± 3.3, p = 0.01; (Nkx2.1/NeuN)$_{WT}$ = 64.7 ± 1.5, (Nkx2.1/NeuN)$_{Lmo3-/-}$ = 49.4 ± 1.2, p = 0.001; two-tailed t tests. The Npas1/NeuN ratio in the mutant also appears increased compared to that of the WT. The percent of Npas1$^+$ neurons expressing FoxP2 appeared slightly higher in the mutants (WT = 58.2 ± 6.4 %, *Lmo3*$_{-/-}$ = 64 ± 2.3 %, 5 sections from 2 brains for WT and 6 sections from 2 brains for *Lmo3*-null), as did the percent of Npas1$^+$ neurons expressing PV (WT = 4 ± 0.4 %, *Lmo3*$_{-/-}$ = 12.1 ± 10 %, 4 sections from 2 brains for WT and 5 sections from 2 brains for *Lmo3*-null), though we did not analyze enough brains to reach statistically significant conclusions for these specific data.

Loss of Lmo3 results in a reduction of the pallidosubthalamic input

The reciprocally connected GPe and subthalamic nucleus (STN) network is integral to basal ganglia function and the pallidal projection to the STN strongly influences and patterns the activity of STN neurons (Bevan et al., 2002; Baufreton et al., 2005, 2009; Atherton et al., 2013). PV$^+$ neurons constitute the major pallidal input to the STN (Hoover and Marshall, 1999; Mallet et al., 2012; Mastro et al., 2014; Abdi et al., 2015; Hernández et al., 2015; Abecassis et al., 2020; Pamukcu et al., 2020). Since PV$^+$ neurons are reduced in the *Lmo3*-null mutants, we wanted to determine if the pallidosubthalamic input is also reduced in the mutants. The pallidosubthalamic projection forms the main GABAergic input to the

STN (Canteras et al., 1990; Smith et al., 1998; Glajch et al., 2016). Thus, we performed immunostaining at P30 for vesicular GABA transporter (vGAT), a marker of GABAergic axon terminals (McIntire et al., 1997), and the presynaptic active zone protein Bassoon (Tom Dieck et al., 1998). Visual inspection of synaptic marker staining in the STN of mutant sections suggested a considerable reduction in size of the STN; thus, we first quantified the area labeled by vGAT and Bassoon immunostaining in the STN, using borders demarcated by NeuN (Fig. 5 A -D, A'–D'). This revealed a significant reduction in area in the *Lmo3*-null mutants compared to wildtype (WT = 1.36 ± 0.09 $\times 10^5$ μm^2, *Lmo3*−/− = 0.87 ± 0.02 $\times 10^5$ μm^2, $p = 0.00052$, two-tailed *t* test, $n=5$ for both genotypes; Fig. 5 E). PV immunoreactivity in the STN was also reduced to a similar extent in the *Lmo3*-null mutants (WT = 1.26 ± 0.03 $\times 10^5$ μm^2, *Lmo3*−/− = 0.8 ± 0.08 $\times 10^5$ μm^2, $n=2$ for both genotypes; Fig. 5 F–J, F'–J'). This PV immunostaining primarily represents pallidosubthalamic axon terminals as *in situ hybridization* data indicate that PV^+ STN neurons are found in a restricted, dorsolateral domain of the structure (Wallén-Mackenzie et al., 2020; Jeon et al., 2022), and cell body staining in the STN was not visible, unlike in the adjacent zona incerta (Fig. 5 H,I'). Importantly, Lmo3 expression has not been reported in studies that have analyzed gene expression in developing STN neurons at embryonic ages (López-González et al., 2021), or in the STN of juvenile (P28) mice (Wallén-Mackenzie et al., 2020) (see also Supplementary Fig. S1).

In addition, we employed a previously established approach (Fan et al., 2012; Chu et al., 2015) to analyze the density of inhibitory presynaptic structures in the STN, in order to assess if there were any changes in the *Lmo3*-null. From high magnification confocal images, we counted $vGAT^+$ structures, as well as $Bassoon^+$ structures that colocalized with $vGAT^+$ structures, using an optical dissector method. However, this analysis did not reveal any changes in the density of $vGAT^+$ or $Bassoon^+$;$vGAT^+$ structures in the *Lmo3*-null, as compared to WT ($vGAT_{WT}$ = 41.02, 30.81 – 45.59 million/mm^3, $vGAT_{Lmo3-/-}$ = 37.51, 25.55 – 43.78 million/mm^3, $p = 0.193$, Mann-Whitney *U* test, $n=8$ for both genotypes; and Bassoon;$vGAT_{WT}$ = 44.2, 30.42 – 69.16 million/mm^3, Bassoon;$vGAT_{Lmo3-/-}$ = 37.05, 27.73 – 55.51 million/mm^3, $p = 0.5221$, Mann-Whitney *U* test, $n=7$ for both genotypes; Fig. 5 K, L, K', L', M). The median and range of values for $vGAT^+$ structures in the WT is consistent with an earlier study (Chu et al., 2015). The density of STN neurons, quantitated from the same regions within the STN as inhibitory presynaptic markers, did not display significant differences between the mutants and WT (WT = 0.49 ± 0.05 million $NeuN^+$ cells/mm^3, *Lmo3*−/− = 0.57 ± 0.03 million $NeuN^+$ cells/mm^3, $p = 0.2126$, two-tailed *t* test, $n=8$ for both genotypes). However, we cannot rule out non-cell autonomous effects of the reduced pallidosubthalamic input on the survival of STN neurons and thus the overall size of the STN in *Lmo3*-null mutants, given that afferent input has been shown to be required for neuronal survival in other regions of the brain (Kim and Sun, 2011; Bathina and Das, 2015).

Loss of Lmo3 does not affect the development of cholinergic GPe neurons and striatal projection neurons

Lmo3 is expressed broadly in regions of the developing subpallium (Fig. 1) that are the source of several basal ganglia neuronal subtypes, in addition to GABAergic GPe projection neurons. Cholinergic neurons form a relatively small proportion of the GPe and project to

the frontal cortex (Saunders et al., 2015; Abecassis et al., 2020). These cholinergic neurons arise primarily from the MGE (Flandin et al., 2010; Nóbrega-Pereira et al., 2010). We examined the *Lmo3*-null mutants for changes in the development of cholinergic neurons by performing immunostaining for choline acetyl transferase (ChAT) and found no significant differences between controls and *Lmo3*-null mutants in $ChAT^+$ neurons along the border of the GPe and the nucleus basalis (Supplementary Fig. S2 A, A', G). Other cholinergic neuron subtypes: striatal $ChAT^+$ interneurons and $ChAT^+$ projection neurons in the septum and diagonal band that also arise from the MGE (Olsson et al., 1998; Marín et al., 2000; Zhao et al., 2003), were also not altered in the *Lmo3*-nulls: see (Fig. S2 B,C,D,E, B',C',D',E', H) for striatal $ChAT^+$ interneurons, and (Fig. S2 F, F′) for $ChAT^+$ projection neurons in the septum and diagonal band. Striatal spiny projection neurons (SPNs) are born in the LGE (Olsson et al., 1998; Wichterle et al., 2001). Immunostaining for dopamine- and cAMP-regulated neuronal phosphoprotein 32 (DARPP-32), a marker for all SPNs (Anderson and Reiner, 1991), revealed no gross changes in the development of SPNs of the striatum as judged by the normal innervation of targets by projection neurons of both the direct and indirect pathway (Fig. S2 I–K, I'-K').

Reduction of MGE derived neurons in the *Lmo3* null GPe is evident at birth

We next sought to determine whether we could observe neuronal subtype specific changes seen in the GPe of mature *Lmo3*-null mice, at earlier time points. Since *Lmo3* is strongly expressed in the SVZ of the MGE as well as the developing GPe during embryonic time points when GPe neurons are born (Fig. 1) and (Marchand and Lajoie, 1986; Nóbrega-Pereira et al., 2010); we hypothesized that Lmo3 is required during embryonic time points for correct cell fate specification in the GPe. We thus analyzed the control and *Lmo3*-null GPe at P0. Since GPe neurons do not express detectable levels of PV until at later postnatal stages (Mitrofanis, 1992), we performed *in situ* hybridization for Er81, a transcription factor that is expressed in most PV^+ neurons in the adult GPe (Nóbrega-Pereira et al., 2010) and found that *Er81* expression is strongly reduced in the GPe of P0 *Lmo3*-null mice as compared to controls (Fig. 6 A–F). In addition, we also performed immunohistochemistry for Nkx2.1 and FoxP2 (Fig. 6 G–L). In the mutant, $Nkx2.1^+$ neuron number was reduced ($rostral_{WT}$ = 738 ± 2, $rostral_{Lmo3-/-}$ = 500.9 ± 13.4, p = 0.0032; $caudal_{WT}$ = 431.1 ± 48.7, $caudal_{Lmo3-/-}$ = 203.4 ± 22.3; p = 0.03; two-tailed t test, n=3 for both genotypes; Fig. 6 N) whereas the numbers of $FoxP2^+$ neurons were unaltered compared to control ($rostral_{WT}$ = 231.3 ± 28.3, $rostral_{Lmo3-/-}$ = 253.6 ± 46.4, p = 0.709; $caudal_{WT}$ = 221.6 ± 12.4, $caudal_{Lmo3-/-}$ = 267.7 ± 33.4; p = 0.324; two-tailed t test, n=3 for both genotypes; Fig. 6 N) The number of $Nkx2.1^+$ neurons in both the WT and *Lmo3*-null is higher at P0 than at P30 (compare Fig. 3 I,J,K to Fig. 6 N), which is likely due to the fact that $Npas1^+$ neurons progressively downregulate Nkx2.1 expression postnatally (Flandin et al., 2010; Abdi et al., 2015; Dodson et al., 2015; Abecassis et al., 2020).

Analysis of *Lmo3* null mice at embryonic time points

The fact that $Nkx2.1^+$ neurons and *Er81* expression in the *Lmo3*-null mutants are already reduced at P0 supports the idea that Lmo3 is required during prenatal stages for the development of GPe neurons. To assess whether reduced proliferation may contribute to this phenotype, we assessed phospho-histone 3 (pH3) expressing (M-phase) cells in the

MGE of E11.5, E12.5 and E13.5 controls and *Lmo3*-null mutants. We calculated the density of $pH3^+$ cells in the ventricular zone and subventricular zone of the ventral MGE which is the source of PV^+ and $Nkx2.1^+$ GPe neurons (Flandin et al., 2010; Nóbrega-Pereira et al., 2010), but found no significant difference between controls and mutants in either the caudal or rostral MGE; density of $pH3^+$ cells in the PoA which is the source of a small fraction of PV^+ and $Nkx2.1^+$ GPe neurons (Nóbrega-Pereira et al., 2010; Abecassis et al., 2020), was also unchanged in the mutants (Supplementary Fig. S3). Staining for the apoptosis marker activated caspase-3 revealed no overt changes in the density of $Casp3^+$ cells between the MGE of controls and *Lmo3*-null mutants at E12.5, E13.5, or the GPe of controls and mutants at P0 (Supplementary Fig. S4), while migration of β-galactosidase expressing cells to the GPe appears grossly normal in the mutants as compared to *Lmo3*+/− mice (Supplementary Fig. S5 A,B,C,D).

GPe development has been shown to depend on transcription factors that control ventral telencephalon patterning and differentiation, such as Dlx2 and Mash1 (Long et al., 2009a, 2009b; Nóbrega-Pereira et al., 2010), and Nkx2.1, which is a primary determinant of MGE identity and is also required at later stages of development of MGE derived neurons like cortical and striatal interneurons (Sussel et al., 1999; Du et al., 2008; Butt et al., 2008). We thus analyzed the expression of these genes in the *Lmo3* mutants at E13.5. However, as shown in Fig. 7, loss of Lmo3 does not alter the expression of these transcription factors. The LIM-HD gene *Lhx6*, a transcriptional target of Nkx2.1 (Du et al., 2008), is required for the differentiation, but not subtype specification, of MGE derived cortical interneurons (Liodis et al., 2007; Du et al., 2008), while *Lhx6* and *Lhx8* double mutants have defects in GPe development (Flandin et al., 2011). Expression of these genes was also unchanged in the *Lmo3*-null mutants (Fig. 8), which is in line with the fact that they are likely upstream of Lmo3 in development (Flandin et al., 2011). In addition, the *Lmo3*null mutant displayed no changes in the expression patterns of *Lmo4* and *Pax6* (Fig. 8), which are markers for the LGE (Flandin et al., 2010; Long et al., 2009b; Stoykova et al., 2000).

Both PV^+ GPe projection neurons and PV^+ cortical interneurons arise from the MGE, although PV^+ cortical interneurons are generated over a more protracted time frame as compared to PV^+ GPe neurons (Miyoshi et al., 2007; Nóbrega-Pereira et al., 2010; Inan et al., 2012). In addition, PV^+ GPe neurons arise from a more caudoventral region of the MGE as compared to PV^+ cortical interneurons (Flandin et al., 2010; Inan et al., 2012; Nóbrega-Pereira et al., 2010). Since *Lmo3*-null mutants also have reduced numbers of PV^+ cortical interneurons (Au et al., 2013), we next analyzed genes that show expression gradients along the rostrocaudal and dorsoventral axes of the MGE, and/or are involved in the specification of MGE derived cortical interneuron subtypes, such as *Er81*, *Couptf1* and the Sonic Hedgehog (Shh) signaling effectors Gli1 and Ptc1 (Flames et al., 2007; Wonders et al., 2008; Nóbrega-Pereira et al., 2010; Xu et al., 2010; Flandin et al., 2011; Lodato et al., 2011; Hu et al., 2017). Expression patterns of *Er81*, *Couptf1*, *Gli1* and *Ptc1* appeared to be unaltered in the ventral telencephalon of the *Lmo3* null mutants (Fig. 9). Expression patterns of several of the above genes (*Dlx2, Couptf1, Er81, Pax6*) were also analyzed at E12.5, with similar results as above.

Discussion

Studies over the past decade have delineated different subtypes of GABAergic GPe projection neurons based on molecular characteristics, connectivity patterns and functional criteria, which has improved our understanding of the role of the GPe in regulating motor function and dysfunction (Mallet et al., 2012; Abdi et al., 2015; Dodson et al., 2015; Hernández et al., 2015; Mallet et al., 2016; Abrahao and Lovinger, 2018; Abecassis et al., 2020; Pamukcu et al., 2020; Aristieta et al., 2021; Ketzef and Silberberg, 2021; Cui et al., 2021a). However, not much is known about the molecular mechanisms that underlie the development of these GPe neuronal subtypes. Our results demonstrate that Lmo3 is required for the development of MGE derived PV^+ and $Nkx2.1^+$ GPe neurons, but not LGE derived $FoxP2^+$ neurons or cholinergic neurons. Development of SPNs appears normal in *Lmo3*-null mutants. As a consequence of the reduction in PV^+ neurons, *Lmo3*-null mice have a reduced GPe projection to the STN.

There can be differences within a GPe neuronal subpopulation expressing the same molecular marker. For example, the use of transgenic reporter lines driven by subpallial enhancer elements has shown that there are at least two pools of PV^+ neuron progenitors in the MGE: one that generates predominantly rostral PV^+ neurons, and the other, rostral and caudal neurons but with a bias to the latter (Silberberg et al., 2016). In agreement with this, single-cell transcriptomics analysis confirms the existence of two PV^+ neuron clusters within the GPe (Saunders et al., 2018), while a recent study suggested subtle differences in behavior controlled by the two PV^+ neuronal subtypes belonging to these two clusters (Cui et al., 2021b). In light of these observations, it is interesting that the loss of Lmo3 results in a more severe reduction of caudal GPe PV^+ neurons than at rostral and middle levels (Fig. 2 J,K,L). An earlier study showing that PV^+ cortical interneurons but not somatostatin expressing (Sst^+) cortical interneurons (both of which are MGE derived) are reduced upon loss of Lmo3 (Au et al., 2013), also suggests that Lmo3 has a role in the development of specific neuronal subtypes within the MGE. Although $Npas1^+$;$Nkx2.1^+$ neurons form a small proportion (~10%) of GPe neurons, they constitute the non-cholinergic GPe projection to the cortex; densely innervating deep layers of the primary motor and somatosensory cortices (Abecassis et al., 2020). Upon loss of Lmo3, the overall number of $Npas1^+$ neurons is unchanged, but there is a ~ 30% reduction of $Npas1^+$;$Nkx2.1^+$ neurons, and a lower percentage of $Npas1^+$ neurons coexpress Nkx2.1 (Fig. 4). It would be interesting to determine if the latter subpopulation in the mutant retains the same anatomical properties as wildtype $Npas1^+$;$Nkx2.1^+$ GPe neurons, like projecting to the cortex. Lhx6 is another marker for some MGE derived GPe neurons: different subpopulations of $Lhx6^+$ GPe neurons coexpress either PV or Npas1; although there is a small subpopulation of $Lhx6^+$ neurons that expresses neither PV nor Npas1 (Mastro et al., 2014; Dodson et al., 2015; Hernández et al., 2015; Abrahao and Lovinger, 2018; Abecassis et al., 2020). $Lhx6^+$ neurons have electrophysiological properties typically in between the extremes of PV^+ and $FoxP2^+$ neurons, with projections to other basal ganglia structures more similar to PV^+ neurons than $FoxP2^+$ neurons (Mastro et al., 2014; Hernández et al., 2015; Abrahao and Lovinger, 2018; Abecassis et al., 2020). It would be interesting to address whether $Lhx6^+$;PV^+, $Lhx6^+$;$Npas1^+$ and $Lhx6^+$;PV^- ;$Npas1^-$ GPe neurons are spared upon loss of Lmo3 in future

experiments, employing the transgenic mouse line used in the studies mentioned above, for consistency.

While we have shown that loss of Lmo3 results in a reduction of MGE derived GPe neurons by birth, analysis of the *Lmo3*-null mutants at embryonic ages did not reveal any obvious underlying mechanism for the cell subtype specific requirement for Lmo3 in their development. Expression of transcription factors implicated in earlier stages of ventral telencephalon patterning, like *Dlx2*, *Mash1*, *Nkx2.1*, were unaffected in the *Lmo3*-null. The expression of several genes that are expressed in gradients along the rostrocaudal and dorsoventral axes of the MGE (*Couptf1, Gli1, Ptc1*, *Er81)*, and genes that have been shown to influence the development of PV^+ expressing neurons (*Couptf1, Gli1, Ptc1)* in earlier studies (Flames et al., 2007; Xu et al., 2010; Lodato et al., 2011) was also unaffected in the *Lmo3*-null mutant. A shortcoming of our study is that we have not analyzed late embryonic ages for increased cell death in the mutants, which could potentially contribute to the reduction of MGE derived GPe neurons, given that the number of β-galactosidase expressing cells (and the number of $NeuN^+$ cells) is reduced in the GPe of Lmo3 mutants as compared to *Lmo3*+/− mice (Supplementary Fig. S5 J). Another possibility is that Lmo3 could be involved in the regulation of neuron-glia cell fate decisions, given that progenitors in the E11.5 and E12.5 VZ and SVZ of the MGE can also give rise to ventral and dorsal telencephalon oligodendrocytes (Petryniak et al., 2007; Flandin et al., 2010), and because some β-gal expressing cells in the GPe of *Lmo3*+/− mice and *Lmo3*−/− mice do not express NeuN (Fig. S5 H,H',H",I,I',I",J). Interestingly, the related LIM-HD gene *Lhx2* is involved in suppressing astrogliogenesis and promoting neurogenesis in the developing hippocampus (Subramanian et al., 2011).

Functional significance

Our data show a significant reduction of area innervated by GPe axon terminals in the STN of *Lmo3*-null mutants. Similar to this, an earlier study that had investigated the role of the transcription factor Isl1 (which belongs to the same protein family as Lmo3) in the development of striatonigral neurons, showed that striatonigral neurons are reduced in *Isl1* knockout mutants, leading to a considerable reduction in their area of innervation of the EP and SNr (Ehrman et al., 2013). We performed the quantitation of synaptic marker density from roughly the center of the STN in all sections analyzed in both genotypes, and did not any significant change in the *Lmo3*-null, as compared to WT. Nonetheless, an aspect of future work could be functional experiments to determine if GPe-STN synaptic transmission is altered in *Lmo3*-null mutants, and at adult ages in addition to juvenile time points.

Collectively, recent studies indicate that a major function of PV^+ neurons and many $Nkx2.1^+$ neurons, is what was traditionally ascribed to the GPe as a whole. As part of the indirect pathway of the basal ganglia, they receive strong inhibitory input from indirect pathway striatal projection neurons (iSPNs) (Aristieta et al., 2021; Ketzef and Silberberg, 2021; Cui et al., 2021a); a decrease in their firing would disinhibit the STN as well as basal ganglia output nuclei (SNr) in which the axons of many PV^+ and $Nkx2.1^+$ neurons also collateralize, thus suppressing movement (Mallet et al., 2012; Sano et al., 2013); and optogenetic activation of PV^+ neurons and their terminals in the STN has been shown to

promote movement (Pamukcu et al., 2020). The firing of FoxP2$^+$ and Npas1$^+$ neurons would depend on how they integrate input from various sources: motor cortex, dSPNs, iSPNs, STN as well as from PV$^+$ neurons (Mallet et al., 2012; Karube et al., 2019; Aristieta et al., 2021; Ketzef and Silberberg, 2021; Cui et al., 2021a). As regards their role in locomotor behavior, activation of FoxP2$^+$ neurons has been linked to cancellation of ongoing or imminent action (Mallet et al., 2016; Aristieta et al., 2021) while activation of Npas1$^+$ neurons as well as FoxP2$^+$ neurons decreased movement speed and increased the length of time mice spent motionless (Glajch et al., 2016; Pamukcu et al., 2020; Cui et al., 2021b). These behaviors are likely mediated through the dense axonal projections of these neurons to striatal SPNs. Given the above, we could speculate that the reduced PV$^+$ and Nkx2.1$^+$ neurons and pallidosubthalamic input in *Lmo3*-null mice, along with potentially reduced PV$^+$ and Nkx2.1$^+$ inhibitory input to FoxP2$^+$ neurons whose development remains unaffected, would result in reduced motor activity. Data from two studies support this hypothesis: overall locomotor activity was shown to be reduced in *Lmo3*-null mice compared with wildtype controls, and this effect could not be attributed to the function of Lmo3 in the brain regions and behaviors under investigation in those studies- i.e., amygdala and anxiety-like behavior (Savarese and Lasek, 2018; Reisinger et al., 2020).

Optogenetic stimulation of PV$^+$ GPe neurons has been shown to rescue motor deficits in 6-OHDA lesioned mouse models of PD in studies from several laboratories (Pamukcu et al., 2020; Lilascharoen et al., 2021) and a study that used a novel deep brain stimulation (DBS) protocol to drive neuronal subtype-specific neuromodulation in the GPe by harnessing differences in the properties of PV$^+$ and Lhx6$^+$ GPe neurons, achieved longer lasting therapeutic effects than that obtained using a conventional DBS protocol, in an acute 6-OHDA lesioned mouse model (Spix et al., 2021). Such progress underlines the importance of understanding the organization of basal ganglia structures, including molecular factors that control their development.

Supplementary Material

Refer to Web version on PubMed Central for supplementary material.

FUNDING SOURCES:

This work was supported by The National Institutes of Health EY026614 to L.G., the Research to Prevent Blindness challenge grant to the Department of Ophthalmology at the University of Rochester, NIMH R01 MH081880 to J.L.R. and NIH R01 NS069777 to C.S.C.

References

Abdi A, Mallet N, Mohamed FY, Sharott A, Dodson PD, Nakamura KC, Suri S, Avery SV, Larvin JT, Garas FN, Garas SN, Vinciati F, Morin S, Bezard E, Baufreton J, Magill PJ, 2015. Prototypic and arkypallidal neurons in the dopamine-intact external globus pallidus. J. Neurosci. 35, 6667–6688. 10.1523/JNEUROSCI.4662-14.2015 [PubMed: 25926446]

Abecassis ZA, Berceau BL, Win PH, García D, Xenias HS, Cui Q, Pamukcu A, Cherian S, Hernández VM, Chon U, Lim BK, Kim Y, Justice NJ, Awatramani R, Hooks BM, Gerfen CR, Boca SM, Chan CS, 2020. Npas1+−Nkx2.1+ Neurons Are an Integral Part of the Cortico-pallido-cortical Loop. J. Neurosci. 40, 743–768. 10.1523/JNEUROSCI.1199-19.2019 [PubMed: 31811030]

Abrahao KP, Lovinger DM, 2018. Classification of GABAergic neuron subtypes from the globus pallidus using wild-type and transgenic mice. J. Physiol. 596, 4219–4235. 10.1113/JP276079 [PubMed: 29917235]

Anderson KD, Reiner A, 1991. Immunohistochemical localization of DARPP-32 in striatal projection neurons and striatal interneurons: implications for the localization of D1-like dopamine receptors on different types of striatal neurons. Brain Res. 568, 235–243. 10.1016/0006-8993(91)91403-N [PubMed: 1839966]

Aristieta A, Barresi M, Azizpour Lindi S, Barrière G, Courtand G, de la Crompe B, Guilhemsang L, Gauthier S, Fioramonti S, Baufreton J, Mallet NP, 2021. A Disynaptic Circuit in the Globus Pallidus Controls Locomotion Inhibition. Curr. Biol. 31, 707–721.e7. 10.1016/j.cub.2020.11.019 [PubMed: 33306949]

Atherto JF., Menar A., Urbai N., Beva MD., 2013. Short-term depression of external globus pallidus-subthalamic nucleus synaptic transmission and implications for patterning subthalamic activity. J. Neurosci. 33, 7130–7144. 10.1523/JNEUROSCI.3576-12.2013 [PubMed: 23616523]

Au E, Ahmed T, Karayannis T, Biswas S, Gan L, Fishell G, 2013. A modular gain-of-function approach to generate cortical interneuron subtypes from ES cells. Neuron 80, 1145–1158. 10.1016/j.neuron.2013.09.022 [PubMed: 24314726]

Bathina S, Das UN, 2015. Brain-derived neurotrophic factor and its clinical Implications. Arch. Med. Sci. 11, 1164–1178. 10.5114/aoms.2015.56342 [PubMed: 26788077]

Baufreton J, Atherton JF, Surmeier DJ, Bevan MD, 2005. Enhancement of excitatory synaptic integration by GABAergic inhibition in the subthalamic nucleus. J. Neurosci. 25, 8505–8517. 10.1523/JNEUROSCI.1163-05.2005 [PubMed: 16162932]

Baufreton J, Kirkham E, Atherton JF, Menard A, Magill PJ, Bolam JP, Bevan MD, 2009. Sparse but selective and potent synaptic transmission from the globus pallidus to the subthalamic nucleus. J. Neurophysiol. 102, 532–545. 10.1152/jn.00305.2009 [PubMed: 19458148]

Bevan MD, 1998. Selective innervation of neostriatal interneurons by a subclass of neuron in the globus pallidus of the rat. J. Neurosci. 18, 9438–9452. 10.1523/jneurosci.18-22-09438.1998 [PubMed: 9801382]

Bevan MD, Magill PJ, Terman D, Bolam JP, Wilson CJ, 2002. Move to the rhythm: Oscillations in the subthalamic nucleus-external globus pallidus network. Trends Neurosci. 25, 525–531. 10.1016/S0166-2236(02)02235-X [PubMed: 12220881]

Breedveld GJ., Van Dongen JWF., Danesino C., Guala A., Percy AK., Dure LS., Harper P., Lazarou LP., Van Der Linde H., Joosse M., Grüters A., MacDonald ME., De Vries BBA., Arts WFM., Oostra BA., Krude H., Heutink P., 2002. Mutations in TITF-1 are associated with benign hereditary chorea. Hum. Mol. Genet. 11, 971–979. 10.1093/hmg/11.8.971 [PubMed: 11971878]

Bulchand S, Subramanian L, Tole S, 2003. Dynamic spatiotemporal expression of LIM genes and cofactors in the embryonic and postnatal cerebral cortex. Dev. Dyn. 226, 460–469. 10.1002/dvdy.10235 [PubMed: 12619132]

Butt SJB, Sousa VH, Fuccillo MV, Hjerling-Leffler J, Miyoshi G, Kimura S, Fishell G, 2008. The Requirement of Nkx2–1 in the Temporal Specification of Cortical Interneuron Subtypes. Neuron 59, 722–732. 10.1016/j.neuron.2008.07.031 [PubMed: 18786356]

Canteras NS, Shammah-Lagnado SJ, Silva BA, Ricardo JA, 1990. Afferent connections of the subthalamic nucleus: a combined retrograde and anterograde horseradish peroxidase study in the rat. Brain Res. 513, 43–59. 10.1016/0006-8993(90)91087-W [PubMed: 2350684]

Chan CS, Glajch KE, Gertler TS, Guzman JN, Mercer JN, Lewis AS, Goldberg AB, Tkatch T, Shigemoto R, Fleming SM, Chetkovich DM, Osten P, Kita H, Surmeier DJ, 2011. HCN channelopathy in external globus pallidus neurons in models of Parkinson's disease. Nat. Neurosci. 14, 85–94. 10.1038/nn.2692 [PubMed: 21076425]

Chu HY, Atherton JF, Wokosin D, Surmeier DJ, Bevan MD, 2015. Heterosynaptic regulation of external globus pallidus inputs to the subthalamic nucleus by the motor cortex. Neuron 85, 364–376. 10.1016/j.neuron.2014.12.022 [PubMed: 25578364]

Cooper AJ., Stanford IM., 2000. Electrophysiological and morphological characteristics of three subtypes of rat globus pallidus neurone in vitro. J. Physiol. 527, 291–304. 10.1111/j.1469-7793.2000.t01-1-00291.x [PubMed: 10970430]

Courtney CD, Pamukcu A, Chan CS, 2023. Cell and circuit complexity of the external globus pallidus. Nat. Neurosci. 10.1038/s41593-023-01368-7

Courtney CD, Pamukcu A, Chan CS, 2021. The external pallidum: think locally, act globally.

Cui Q, Du X, Chang IYM, Pamukcu A, Lilascharoen V, Berceau BL, García D, Hong D, Chon U, Narayanan A, Kim Y, Lim BK, Chan CS, 2021a. Striatal direct pathway targets Npas1+pallidal neurons. J. Neurosci. 41, 3966–3987. 10.1523/JNEUROSCI.2306-20.2021 [PubMed: 33731445]

Cui Q, Pamukcu A, Cherian S, Chang IYM, Berceau BL, Xenias HS, Higgs MH, Rajamanickam S, Chen Y, Du X, Zhang Y, McMorrow H, Abecassis ZA, Boca SM, Justice NJ, Wilson CJ, Chan CS, 2021b. Dissociable roles of pallidal neuron subtypes in regulating motor patterns. J. Neurosci. 41, 4036–4059. 10.1523/JNEUROSCI.2210-20.2021 [PubMed: 33731450]

DeLong MR, 1971. Activity of pallidal neurons during movement. J. Neurophysiol. 34, 414–427. 10.1152/jn.1971.34.3.414 [PubMed: 4997823]

Dodson PD., Larvin JT., Duffell JM., Garas FN., Doig NM., Kessaris N., Duguid IC., Bogacz R., Butt SJB., Magill PJ., 2015. Distinct developmental origins manifest in the specialized encoding of movement by adult neurons of the external globus pallidus. Neuron 86, 501–513. 10.1016/j.neuron.2015.03.007 [PubMed: 25843402]

Du T, Xu Q, Ocbina PJ, Anderson SA, 2008. NKX2.1 specifies cortical interneuron fate by activating Lhx6. Development 135, 1559–1567. 10.1242/dev.015123 [PubMed: 18339674]

Ehrman LA, Mu X, Waclaw RR, Yoshida Y, Vorhees CV, Klein WH, Campbell K, 2013. The LIM homeobox gene Isl1 is required for the correct development of the striatonigral pathway in the mouse. Proc. Natl. Acad. Sci. U. S. A. 110. 10.1073/pnas.1308275110

Fan KY, Baufreton J, Surmeier DJ, Chan CS, Bevan MD, 2012. Proliferation of external globus pallidus-subthalamic nucleus synapses following degeneration of midbrain dopamine neurons. J. Neurosci. 32, 13718–13728. 10.1523/JNEUROSCI.5750-11.2012 [PubMed: 23035084]

Flames N, Pla R, Gelman DM, Rubenstein JLR, Puelles L, Marín O, 2007. Delineation of multiple subpallial progenitor domains by the combinatorial expression of transcriptional codes. J. Neurosci. 27, 9682–9695. 10.1523/JNEUROSCI.2750-07.2007 [PubMed: 17804629]

Flandin P, Kimura S, Rubenstein JLR, 2010. The progenitor zone of the ventral medial ganglionic eminence requires Nkx2–1 to generate most of the globus pallidus but few neocortical interneurons. J. Neurosci. 30, 2812–2823. 10.1523/JNEUROSCI.4228-09.2010 [PubMed: 20181579]

Flandin P., Zhao Y., Vogt D., Jeong J., Long J., Potter G., Westphal H., Rubenstein JLR., 2011. Lhx6 and Lhx8 Coordinately Induce Neuronal Expression of Shh that Controls the Generation of Interneuron Progenitors. Neuron 70, 939–950. 10.1016/j.neuron.2011.04.020 [PubMed: 21658586]

Gan L, Wang SW, Huang Z, Klein WH, 1999. POU domain factor Brn-3b is essential for retinal ganglion cell differentiation and survival but not for initial cell fate specification. Dev. Biol. 210, 469–480. 10.1006/dbio.1999.9280 [PubMed: 10357904]

Gan L, Xiang M, Zhou L, Wagner DS, Klein WH, Nathans J, 1996. POU domain factor Brn-3b is required for the development of a large set of retinal ganglion cells. Proc. Natl. Acad. Sci. U. S. A. 93, 3920–3925. 10.1073/pnas.93.9.3920 [PubMed: 8632990]

Glajch KE, Kelver DA, Hegeman DJ, Cui Q, Xenias HS, Augustine EC, Hernández VM, Verma N, Huang TY, Luo M, Justice NJ, Chan CS, 2016. Npas1+ pallidal neurons target striatal projection neurons. J. Neurosci. 36, 5472–5488. 10.1523/JNEUROSCI.1720-15.2016 [PubMed: 27194328]

Hegeman DJ, Hong ES, Hernández VM, Chan CS, 2016. The external globus pallidus: Progress and perspectives. Eur. J. Neurosci. 43, 1239–1265. 10.1111/ejn.13196 [PubMed: 26841063]

Hernández VM, Hegeman DJ, Cui Q, Kelver DA, Fiske MP, Glajch KE, Pitt JE, Huang TY, Justice NJ, Savio Chan C, 2015. Parvalbumin + neurons and Npas1 + neurons are distinct neuron classes in the mouse external globus pallidus. J. Neurosci. 35, 11830–11847. 10.1523/JNEUROSCI.4672-14.2015 [PubMed: 26311767]

Hontanilla B., Parent A., Giménez-Amaya JEM., 1994. Compartmental distribution of parvalbumin and calbindin D-28k in rat globus pallidus. Neuroreport 5, 2269–2272. 10.1097/00001756-199411000-00016 [PubMed: 7881043]

Hoover BR, Marshall JF, 1999. Population characteristics of preproenkephalin mRNA-containing neurons in the globus pallidus of the rat. Neurosci. Lett. 265, 199–202. 10.1016/S0304-3940(99)00251-7 [PubMed: 10327165]

Hu JS, Vogt D, Lindtner S, Sandberg M, Silberberg SN, Rubenstein JLR, 2017. CoupTF1 and coup-TF2 control subtype and laminar identity of mge-derived neocortical interneurons. Dev. 144, 2837–2851. 10.1242/dev.150664

Inan M, Welagen J, Anderson SA, 2012. Spatial and temporal bias in the mitotic origins of somatostatin- and parvalbumin-expressing interneuron subgroups and the chandelier subtype in the medial ganglionic eminence. Cereb. Cortex 22, 820–827. 10.1093/cercor/bhr148 [PubMed: 21693785]

Iwahori N, Mizuno N, 1981. A Golgi study on the globus pallidus of the mouse. J. Comp. Neurol. 197, 29–43. 10.1002/cne.901970104 [PubMed: 6164701]

Jeon H, Lee H, Kwon DH, Kim, Jiwon, Tanaka-Yamamoto K, Yook JS, Feng L, Park HR, Lim YH, Cho ZH, Paek SH, Kim, Jinhyun, 2022. Topographic connectivity and cellular profiling reveal detailed input pathways and functionally distinct cell types in the subthalamic nucleus. Cell Rep. 38. 10.1016/j.celrep.2022.110439

Karube F, Takahashi S, Kobayashi K, Fujiyama F, 2019. Motor cortex can directly drive the globus pallidus neurons in a projection neuron type-dependent manner in the rat. Elife 8. 10.7554/eLife.49511

Kepecs A, Fishell G, 2014. Interneuron cell types are fit to function. Nature 505, 318–326. 10.1038/nature12983 [PubMed: 24429630]

Kessaris N., Magno L., Rubin AN., Oliveira MG., 2014. Genetic programs controlling cortical interneuron fate. Curr. Opin. Neurobiol. 26, 79–87. 10.1016/j.conb.2013.12.012 [PubMed: 24440413]

Ketzef M, Silberberg G, 2021. Differential Synaptic Input to External Globus Pallidus Neuronal Subpopulations In Vivo. Neuron 109, 516–529.e4. 10.1016/j.neuron.2020.11.006 [PubMed: 33248017]

Kim WR, Sun W, 2011. Programmed cell death during postnatal development of the rodent nervous system. Dev. Growth Differ. 53, 225–35. 10.1111/j.1440-169X.2010.01226.x [PubMed: 21338348]

Kita H, 2007. Globus pallidus external segment. Prog. Brain Res. 160, 111–133. 10.1016/S0079-6123(06)60007-1 [PubMed: 17499111]

Kita H, 1994. Parvalbumin-immunopositive neurons in rat globus pallidus: a light and electron microscopic study. Brain Res. 657, 31–41. 10.1016/0006-8993(94)90950-4 [PubMed: 7820633]

Kita H, Kitai ST, 1994. The morphology of globus pallidus projection neurons in the rat: an intracellular staining study. Brain Res. 636, 308–319. 10.1016/0006-8993(94)91030-8 [PubMed: 8012814]

Leung C, Jia Z, 2016. Mouse genetic models of human brain disorders. Front. Genet. 7. 10.3389/fgene.2016.00040

Lilascharoen V., Wang EHJ., Do N., Pate SC., Tran AN., Yoon CD., Choi JH., Wang XY., Pribiag H., Park YG., Chung K., Lim BK., 2021. Divergent pallidal pathways underlying distinct Parkinsonian behavioral deficits. Nat. Neurosci. 24, 504–515. 10.1038/s41593-021-00810-y [PubMed: 33723433]

Liodis P, Denaxa M, Grigoriou M, Akufo-Addo C, Yanagawa Y, Pachnis V, 2007. Lhx6 activity is required for the normal migration and specification of cortical interneuron subtypes. J. Neurosci. 27, 3078–3089. 10.1523/JNEUROSCI.3055-06.2007 [PubMed: 17376969]

Lodato S, Tomassy GS, De Leonibus E, Uzcategui YG, Andolfi G, Armentano M, Touzot A, Gaztelu JM, Arlotta P, De La Prida LM, Studer M, 2011. Loss of COUPTFI alters the balance between caudal ganglionic eminence- and medial ganglionic eminence-derived cortical interneurons and results in resistance to epilepsy. J. Neurosci. 31, 4650–4662. 10.1523/JNEUROSCI.6580-10.2011 [PubMed: 21430164]

Long JE, Cobos I, Potter GB, Rubenstein JLR, 2009a. Dlx1&2 and Mash1 transcription factors control MGE and CGE patterning and differentiation through parallel and overlapping pathways. Cereb. Cortex 19. 10.1093/cercor/bhp045

Long JE, Swan C, Liang WS, Cobos I, Potter GB, Rubenstein JLR, 2009b. Dlx1&2 and Mash1 transcription factors control striatal patterning and differentiation through parallel and overlapping pathways. J. Comp. Neurol. 512, 556–572. 10.1002/cne.21854 [PubMed: 19030180]

López-González L, Alonso A, García-Calero E, de Puelles E, Puelles L, 2021. Tangential Intrahypothalamic Migration of the Mouse Ventral Premamillary Nucleus and Fgf8 Signaling. Front. cell Dev. Biol. 9, 676121. 10.3389/fcell.2021.676121 [PubMed: 34095148]

Magill PJ., Bolam JP., Bevan MD., 2001. Dopamine regulates the impact of the cerebral cortex on the subthalamic nucleus-globus pallidus network. Neuroscience 106, 313–330. 10.1016/S0306-4522(01)00281-0 [PubMed: 11566503]

Magnin M, Morel A, Jeanmonod D, 2000. Single-unit analysis of the pallidum, thalamus and subthalamic nucleus in parkinsonian patients. Neuroscience 96, 549–564. 10.1016/S0306-4522(99)00583-7 [PubMed: 10717435]

Mallet N, Micklem BR, Henny P, Brown MT, Williams C, Bolam JP, Nakamura KC, Magill PJ, 2012. Dichotomous Organization of the External Globus Pallidus. Neuron 74, 1075–1086. 10.1016/j.neuron.2012.04.027 [PubMed: 22726837]

Mallet N, Pogosyan A, Márton LF, Bolam JP, Brown P, Magill PJ, 2008. Parkinsonian beta oscillations in the external globus pallidus and their relationship with subthalamic nucleus activity. J. Neurosci. 28, 14245–14258. 10.1523/JNEUROSCI.4199-08.2008 [PubMed: 19109506]

Mallet N, Schmidt R, Leventhal D, Chen F, Amer N, Boraud T, Berke JD, 2016. Arkypallidal Cells Send a Stop Signal to Striatum. Neuron 89, 308–316. 10.1016/j.neuron.2015.12.017 [PubMed: 26777273]

Marchand R, Lajoie L, 1986. Histogenesis of the striopallidal system in the rat. Neurogenesis of its neurons. Neuroscience 17, 573–590. 10.1016/0306-4522(86)90031-X [PubMed: 3703249]

Marín O, Anderson SA, Rubenstein JLR, 2000. Origin and molecular specification of striatal interneurons. J. Neurosci. 20, 6063–6076. 10.1523/jneurosci.20-16-06063.2000 [PubMed: 10934256]

Mastro KJ., Bouchard RS., Holt HAK., Gittis AH., 2014. Transgenic mouse lines subdivide external segment of the globus pallidus (GPe) neurons and reveal distinct GPe output pathways. J. Neurosci. 34, 2087–2099. 10.1523/JNEUROSCI.4646-13.2014 [PubMed: 24501350]

McIntire SL, Reimer RJ, Schuske K, Edwards RH, Jorgensen EM, 1997. Identification and characterization of the vesicular GABA transporter. Nature 389, 870–876. 10.1038/39908 [PubMed: 9349821]

Mitrofanis J, 1992. Patterns of antigenic expression in the thalamic reticular nucleus of developing rats. J. Comp. Neurol. 320, 161–181. 10.1002/cne.903200203 [PubMed: 1377717]

Miyoshi G, Butt SJB, Takebayashi H, Fishell G, 2007. Physiologically distinct temporal cohorts of cortical interneurons arise from telencephalic Olig2-expressing precursors. J. Neurosci. 27, 7786–7798. 10.1523/JNEUROSCI.1807-07.2007 [PubMed: 17634372]

Nambu A, Chiken S, Shashidharan P, Nishibayashi H, Ogura M, Kakishita K, Tanaka S, Tachibana Y, Kita H, Itakura T, 2011. Reduced pallidal output causes dystonia. Front. Syst. Neurosci. 10.3389/fnsys.2011.00089

Nery S, Fishell G, Corbin JG, 2002. The caudal ganglionic eminence is a source of distinct cortical and subcortical cell populations. Nat. Neurosci. 5, 1279–1287. 10.1038/nn971 [PubMed: 12411960]

Nini A, Feingold A, Slovin H, Bergman H, 1995. Neurons in the globus pallidus do not show correlated activity in the normal monkey, but phase-locked oscillations appear in the MPTP model of Parkinsonism. J. Neurophysiol. 74, 1800–1805. 10.1152/jn.1995.74.4.1800 [PubMed: 8989416]

Nóbrega-Pereira S., Gelman D., Bartolini G., Pla R., Pierani A., Marín O., 2010. Origin and molecular specification of globus pallidus neurons. J. Neurosci. 30, 2824–2834. 10.1523/JNEUROSCI.4023-09.2010 [PubMed: 20181580]

Olsson M, Björklund A, Campbell K, 1998. Early specification of striatal projection neurons and interneuronal subtypes in the lateral and medial ganglionic eminence. Neuroscience 84, 867–876. 10.1016/S0306-4522(97)00532-0 [PubMed: 9579790]

Pamukcu A, Cui Q, Xenias HS, Berceau BL, Augustine EC, Fan I, Chalasani S, Hantman AW, Lerner TN, Boca SM, Savio Chan C, 2020. Parvalbumin1 and Npas11 pallidal neurons have distinct

circuit topology and function. J. Neurosci. 40, 7855–7876. 10.1523/JNEUROSCI.0361-20.2020 [PubMed: 32868462]

Pan HS, Walters JR, 1988. Unilateral lesion of the nigrostriatal pathway decreases the firing rate and alters the firing pattern of globus pallidus neurons in the rat. Synapse 2, 650–656. 10.1002/syn.890020612 [PubMed: 3145582]

Petryniak MA, Potter GB, Rowitch DH, Rubenstein JLR, 2007. Dlx1 and Dlx2 control neuronal versus oligodendroglial cell fate acquisition in the developing forebrain. Neuron 55, 417–33. 10.1016/j.neuron.2007.06.036 [PubMed: 17678855]

Pohlenz J, Dumitrescu A, Zundel D, Martiné U, Schönberger W, Koo E, Weiss RE, Cohen RN, Kimura S, Refetoff S, 2002. Partial deficiency of thyroid transcription factor 1 produces predominantly neurological defects in humans and mice. J. Clin. Invest. 109, 469–473. 10.1172/JCI0214192 [PubMed: 11854318]

Reisinger SN., Bilban M., Stojanovic T., Derdak S., Yang J., Cicvaric A., Horvath O., Sideromenos S., Zambon A., Monje FJ., Boehm S., Pollak DD., 2020. Lmo3 deficiency in the mouse is associated with alterations in mood-related behaviors and a depression-biased amygdala transcriptome. Psychoneuroendocrinology 111. 10.1016/j.psyneuen.2019.104480

Sano H, Chiken S, Hikida T, Kobayashi K, Nambu A, 2013. Signals through the striatopallidal indirect pathway stop movements by phasic excitation in the substantia nigra. J. Neurosci. 33, 7583–7594. 10.1523/JNEUROSCI.4932-12.2013 [PubMed: 23616563]

Saunders A, Huang KW, Sabatini BL, 2016. Globus Pallidus Externus Neurons Expressing parvalbumin Interconnect the Subthalamic Nucleus and Striatal Interneurons. PLoS One 11. 10.1371/journal.pone.0149798

Saunders A, Macosko EZ, Wysoker A, Goldman M, Krienen FM, de Rivera H, Bien E, Baum M, Bortolin L, Wang S, Goeva A, Nemesh J, Kamitaki N, Brumbaugh S, Kulp D, McCarroll SA, 2018. Molecular Diversity and Specializations among the Cells of the Adult Mouse Brain. Cell 174, 1015–1030.e16. 10.1016/j.cell.2018.07.028 [PubMed: 30096299]

Saunders A, Oldenburg IA, Berezovskii VK, Johnson CA, Kingery ND, Elliott HL, Xie T, Gerfen CR, Sabatini BL, 2015. A direct GABAergic output from the basal ganglia to frontal cortex. Nature 521, 85–89. 10.1038/nature14179 [PubMed: 25739505]

Savarese A., Lasek AW., 2018. Regulation of anxiety-like behavior and Crhr1 expression in the basolateral amygdala by LMO3. Psychoneuroendocrinology 92, 13–20. 10.1016/j.psyneuen.2018.03.016 [PubMed: 29609111]

Silberberg SN, Taher L, Lindtner S, Sandberg M, Nord AS, Vogt D, Mckinsey GL, Hoch R, Pattabiraman K, Zhang D, Ferran JL, Rajkovic A, Golonzhka O, Kim C, Zeng H, Puelles L, Visel A, Rubenstein JLR, 2016. Subpallial Enhancer Transgenic Lines: a Data and Tool Resource to Study Transcriptional Regulation of GABAergic Cell Fate. Neuron 92, 59–74. 10.1016/j.neuron.2016.09.027 [PubMed: 27710791]

Smith Y, Bevan MD, Shink E, Bolam JP, 1998. Microcircuitry of the direct and indirect pathways of the basal ganglia. Neuroscience 86, 353–387. 10.1016/S0306-4522(98)00004-9 [PubMed: 9881853]

Spix TA, Nanivadekar S, Toong N, Kaplow IM, Isett BR, Goksen Y, Pfenning AR, Gittis AH, 2021. Population-specific neuromodulation prolongs therapeutic benefits of deep brain stimulation. Science (80-.). 374, 201–206. 10.1126/science.abi7852

Starr PA, Kang GA, Heath S, Shimamoto S, Turner RS, 2008. Pallidal neuronal discharge in Huntington's disease: Support for selective loss of striatal cells originating the indirect pathway. Exp. Neurol. 211, 227–233. 10.1016/j.expneurol.2008.01.023 [PubMed: 18342309]

Starr PA, Rau GM, Davis V, Marks WJ, Ostrem JL, Simmons D, Lindsey N, Turner RS, 2005. Spontaneous pallidal neuronal activity in human dystonia: Comparison with Parkinson's disease and normal macaque. J. Neurophysiol. 93, 3165–3176. 10.1152/jn.00971.2004 [PubMed: 15703229]

Stoykova A, Treichel D, Hallonet M, Gruss P, 2000. Pax6 modulates the dorsoventral patterning of the mammalian telencephalon. J. Neurosci. 20, 8042–8050. 10.1523/jneurosci.20-21-08042.2000 [PubMed: 11050125]

Su-Feher L, Rubin AN, Silberberg SN, Catta-Preta R, Lim KJ, Ypsilanti AR, Zdilar I, McGinnis CS., McKinsey GL., Rubino TE., Hawrylycz MJ., Thompson C., Gartner ZJ., Puelles L., Zeng H., Rubenstein JLR., Nord AS., 2022. Single cell enhancer activity distinguishes GABAergic and cholinergic lineages in embryonic mouse basal ganglia. Proc. Natl. Acad. Sci. U. S. A. 119, e2108760119. 10.1073/pnas.2108760119

Subramanian L, Sarkar A, Shetty AS, Muralidharan B, Padmanabhan H, Piper M, Monuki ES, Bach I, Gronostajski RM, Richards LJ, Tole S, 2011. Transcription factor Lhx2 is necessary and sufficient to suppress astrogliogenesis and promote neurogenesis in the developing hippocampus. Proc. Natl. Acad. Sci. U. S. A. 108, E265–74. 10.1073/pnas.1101109108 [PubMed: 21690374]

Sussel L, Marin O, Kimura S, Rubenstein JLR, 1999. Loss of Nkx2.1 homeobox gene function results in a ventral to dorsal molecular respecification within the basal telencephalon: Evidence for a transformation of the pallidum into the striatum. Development 126, 3359–3370. 10.1242/dev.126.15.3359 [PubMed: 10393115]

Tom Dieck S, Sanmartí-Vila L, Langnaese K, Richter K, Kindler S, Soyke A, Wex H, Smalla KH., Kämpf U., Fränzer JT., Stumm M., Garner CC., Gundelfinger ED., 1998. Bassoon, a novel zinc-finger CAG/glutamine-repeat protein selectively localized at the active zone of presynaptic nerve terminals. J. Cell Biol. 142, 499–509. 10.1083/jcb.142.2.499 [PubMed: 9679147]

Tse E, Smith AJH, Hunt S, Lavenir I, Forster A, Warren AJ, Grutz G, Foroni L, Carlton MBL, Colledge WH, Boehm T, Rabbitts TH, 2004. Null Mutation of the Lmo4 Gene or a Combined Null Mutation of the Lmo1 / Lmo3 Genes Causes Perinatal Lethality, and Lmo4 Controls Neural Tube Development in Mice. Mol. Cell. Biol. 24, 2063–2073. 10.1128/mcb.24.5.2063-2073.2004 [PubMed: 14966285]

Waldvogel HJ, Kim EH, Tippett LJ, Vonsattel JPG, Faull RLM, 2014. The neuropathology of Huntington's disease. Curr. Top. Behav. Neurosci. 22, 33–80. 10.1007/7854_2014_354

Walker RH, Arbuthnott GW, Wright AK, 1989. Electrophysiological and anatomical observations concerning the pallidostriatal pathway in the rat. Exp. Brain Res. 74, 303–310. 10.1007/BF00248863 [PubMed: 2494050]

Wallén-Mackenzie Å, Dumas S, Papathanou M, Martis Thiele MM, Vlcek B, König N, Björklund ÅK, 2020. Spatio-molecular domains identified in the mouse subthalamic nucleus and neighboring glutamatergic and GABAergic brain structures. Commun. Biol. 3. 10.1038/s42003-020-1028-8

West MJ, 1999. Stereological methods for estimating the total number of neurons and synapses: Issues of precision and bias. Trends Neurosci. 22, 51–61. 10.1016/S0166-2236(98)01362-9 [PubMed: 10092043]

Wichterle H., Turnbull DH., Nery S., Fishell G., Alvarez-Buylla A., 2001. In utero fate mapping reveals distinct migratory pathways and fates of neurons born in the mammalian basal forebrain. Development 128, 3759–3771. 10.1242/dev.128.19.3759 [PubMed: 11585802]

Wonders CP, Taylor L, Welagen J, Mbata IC, Xiang JZ, Anderson SA, 2008. A spatial bias for the origins of interneuron subgroups within the medial ganglionic eminence. Dev. Biol. 314, 127–136. 10.1016/j.ydbio.2007.11.018 [PubMed: 18155689]

Xu Q, Guo L, Moore H, Waclaw RR, Campbell K, Anderson SA, 2010. Sonic Hedgehog Signaling Confers Ventral Telencephalic Progenitors with Distinct Cortical Interneuron Fates. Neuron 65, 328–340. 10.1016/j.neuron.2010.01.004 [PubMed: 20159447]

Zhao Y, Marín O, Hermesz E, Powell A, Flames N, Palkovits M, Rubenstein JLR, Westphal H, 2003. The LIM-homeobox gene Lhx8 is required for the development of many cholinergic neurons in the mouse forebrain. Proc. Natl. Acad. Sci. U. S. A. 100, 9005–9010. 10.1073/pnas.1537759100 [PubMed: 12855770]

Highlights

- Lmo3 is required for the development of Nkx2.1^{+} and PV^{+} GPe neurons
- *Lmo3*-null mice have reduced inhibitory input to the subthalamic nucleus
- Numbers of FoxP2^{+} GPe neurons are normal in *Lmo3*-null mice
- Expression of key embryonic ventral telencephalon genes unchanged in *Lmo3*-null mice

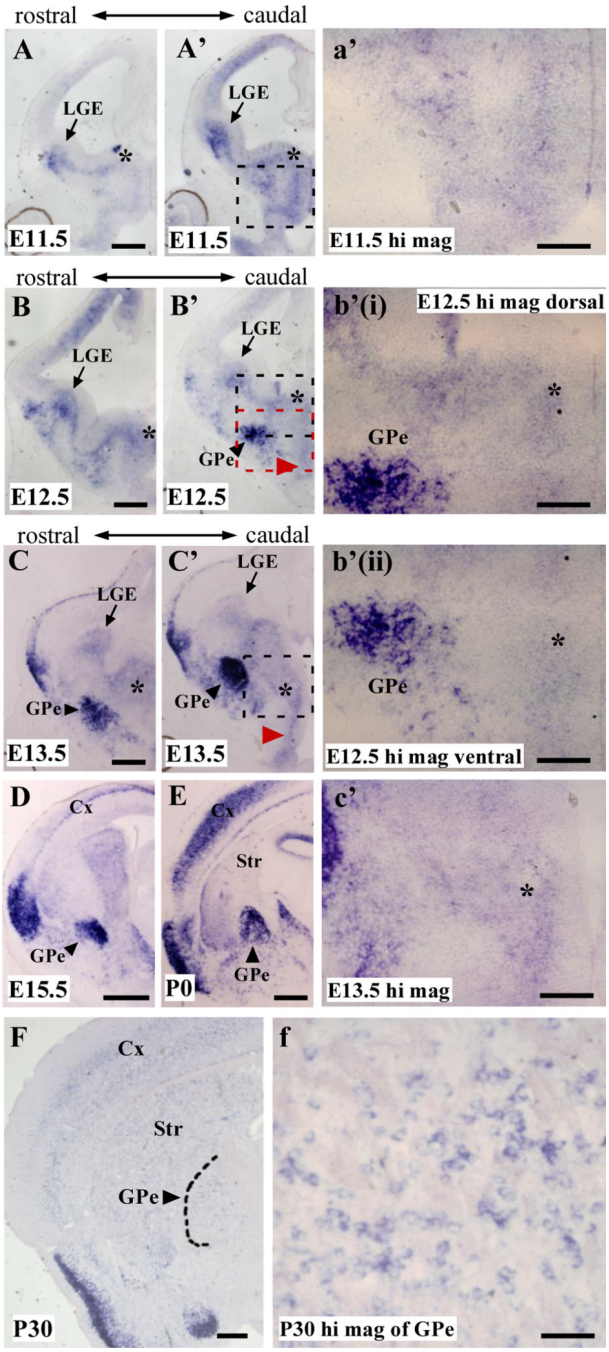

Figure 1.

Lmo3 is expressed in the ganglionic eminences and developing globus pallidus. *Lmo3* is expressed in the SVZ and mantle zone of the LGE (arrows) and MGE (asterisks) in a more rostral (left column) and caudal (right column) level, at E11.5 (**A**, **A'**), E12.5 (**B**, **B'**) and E13.5 (**C**, **C'**), in the SVZ of the PoA (red arrowheads) (**B'**, **C'**) and in the developing GPe (black arrowheads) (**B'**, **C**, **C'**). **a'** is a higher magnification view of the boxed region in **A'**. **b'(i)** and **b'(ii)** are higher magnification views of the dorsal MGE (black box) and ventral MGE and PoA (red box) respectively, in **B'**. (**c'**) is a higher magnification view of

the SVZ of the boxed region in **C'**. **D**, *Lmo3* expression in the developing GPe (arrowhead) at E15.5. **E**, *Lmo3* expression is maintained in the GPe at birth (P0). **F**, *Lmo3* expression is maintained albeit weakly, in the GPe at P30. **f** is a higher magnification view of the GPe in **F**. Abbreviations: Ctx, cortex; GPe, external globus pallidus; Str, striatum; SVZ, subventricular zone. Scale bars: A-C, 500 μm; a'-c',f, D,E, 200 μm; F, 400 μm.

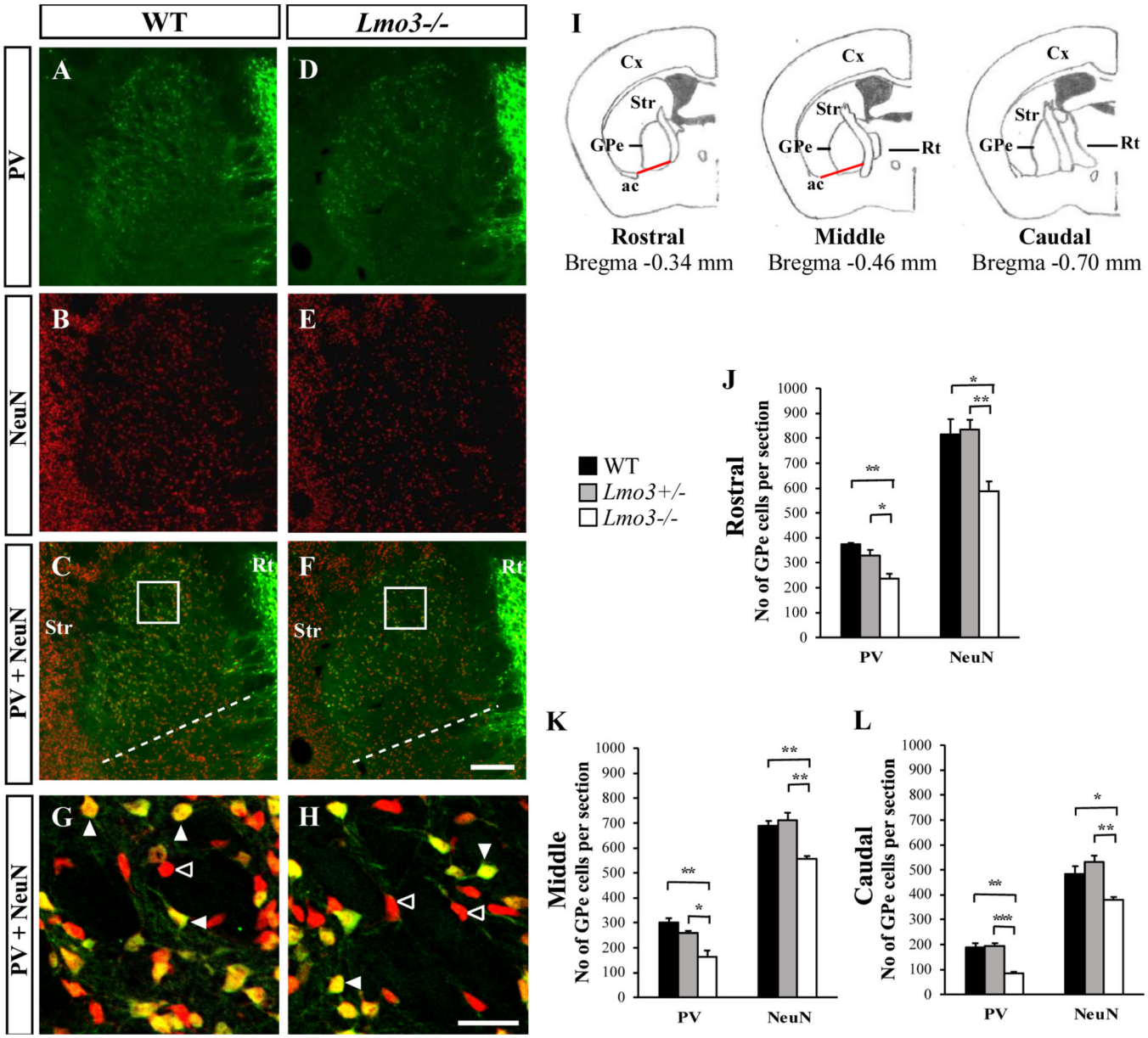

Figure 2.

Lmo3 is required for the development of PV-expressing neurons of the external globus pallidus (GPe). **A-F**, Coronal views of the GPe of P30 wildtype (**A-C**) and *Lmo3*-null mutants (**D-F**) immunostained for parvalbumin (PV) and NeuN. Dashed lines in **C** and **F** indicate the ventral GPe borders used for counting. **G** and **H** are high magnification images of the regions indicated by the boxes in **C** and **F**, respectively. Filled arrowheads indicate PV^+;$NeuN^+$ neurons; open arrowheads indicate neurons that are only $NeuN^+$. **I**, Coronal sections illustrating the rostral, middle and caudal levels of the GPe from which neurons were counted. The ventral GPe borders used for counting were demarcated by the red lines. **J-L**, Graphs displaying the quantification of PV^+ and $NeuN^+$ neurons for the indicated levels. (n=4 for WT and *Lmo3*−/− and n=3 for Lmo3+/−). [Graphs indicate mean values; error bars show SEM. Two-tailed t test, *$p < 0.05$, **$p < 0.01$, ***$p < 0.001$] Scale bars:

(**F**) 200 μm; (**H**) 50 μm. Abbreviations: ac, anterior commissure; Cx, cortex; GPe, external globus pallidus; Rt, reticular nucleus of the thalamus; Str, striatum.

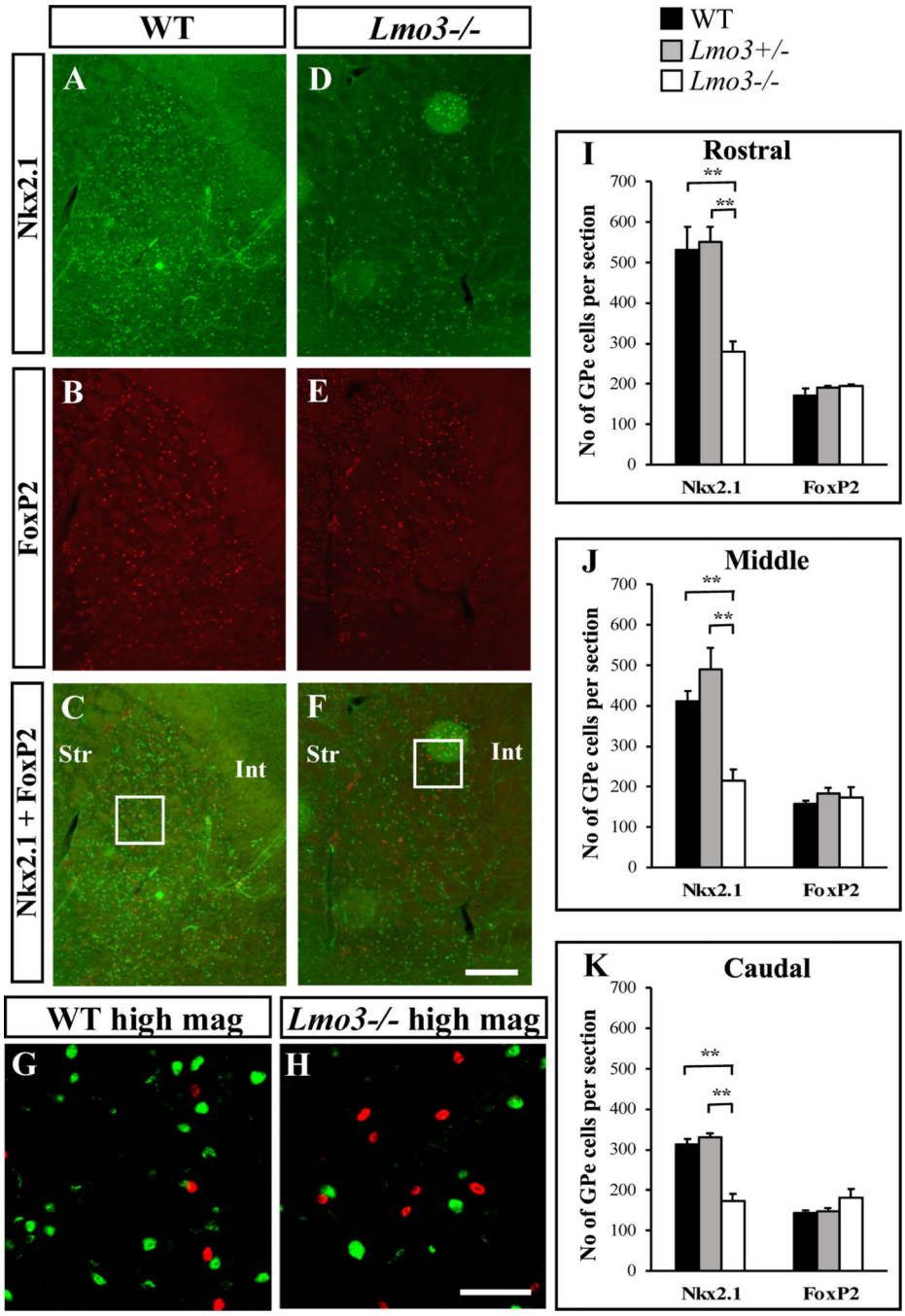

Figure 3.

Nkx2.1^{+} neurons are reduced in the *Lmo3*-null mutant. **A**-**F**, Coronal views of the GPe of P30 wildtype (**A**-**C**) and *Lmo3*-null mutants (**D**-**F**) immunostained for Nkx2.1 and FoxP2. **G** and **H** are high magnification images of the boxed regions in **C** and **F**, respectively. FoxP2 and Nkx2.1 expression is mutually exclusive in both WT and *Lmo3*-null. **I**-**K**, Quantification of Nkx2.1^{+} and FoxP2^{+} GPe neurons from three different rostrocaudal levels (see Fig. 2. n=4 each for WT, *Lmo3*+/− and *Lmo3*−/−). [Graphs indicate mean values; error

bars show SEM. Two-tailed *t* test, *$p < 0.05$, **$p < 0.01$, ***$p < 0.001$] Scale bars: (**F**) 200 μm; (**H**) 50 μm. Abbreviations: Int, internal capsule; Str, striatum.

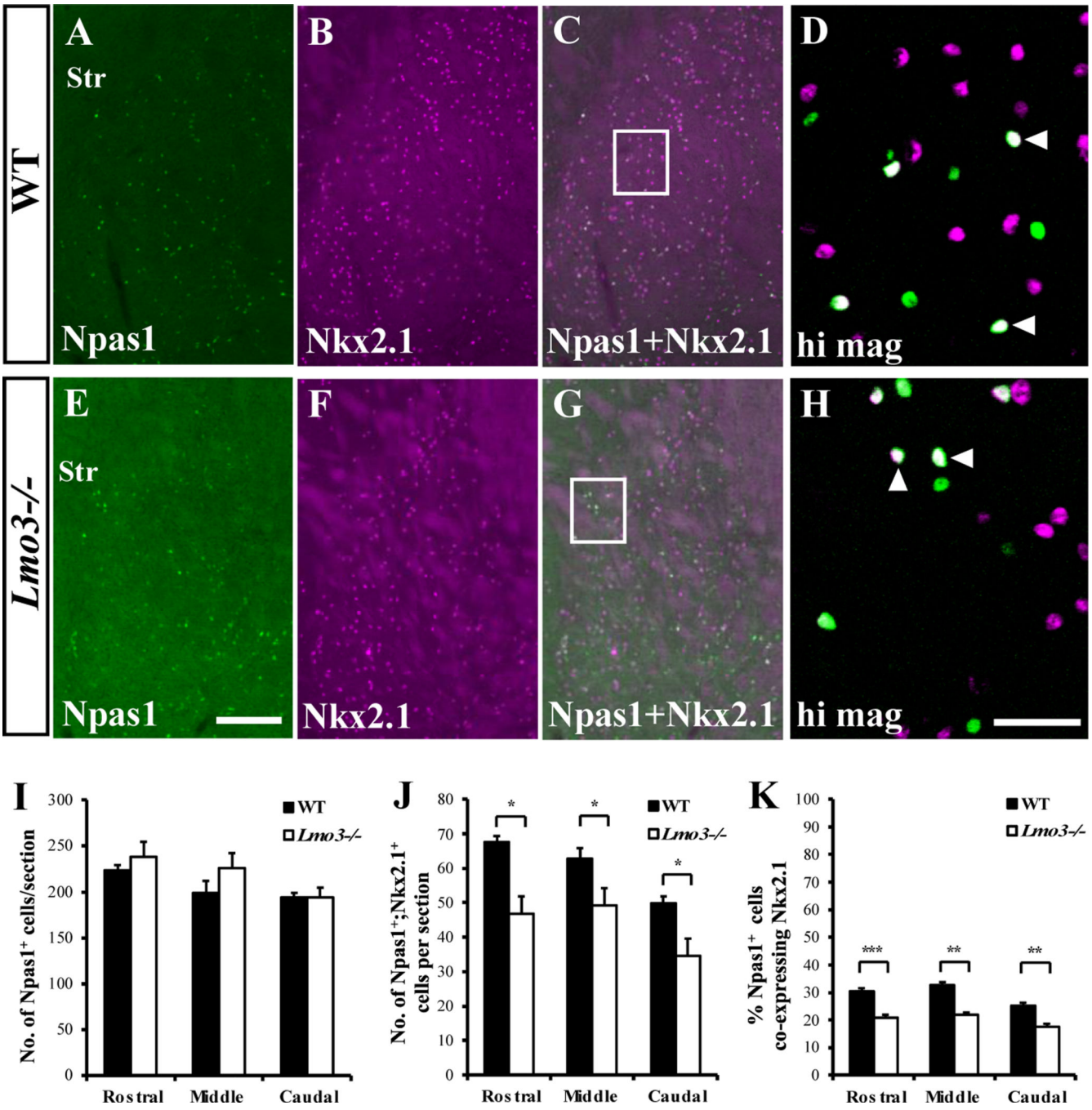

Figure 4.

Npas1$^+$;Nkx2.1$^+$ neurons are reduced in the *Lmo3*-null mutant. Coronal views of the GPe of P30 wildtype (**A**-**C**) and *Lmo3*-null mutants (**E**-**G**) immunostained for Npas1 and Nkx2.1. **D** and **H** are high magnification images of the boxed regions in **C** and **G**, respectively. Filled arrowheads indicate Npas1$^+$;Nkx2.1$^+$ neurons. **I**-**K**, Quantification of Npas1$^+$ (**I**), Npas1$^+$;Nkx2.1$^+$ (**J**) GPe neurons and % Npas1$^+$ neurons coexpressing Nkx2.1$^+$ (**K**) from three different rostrocaudal levels (see Fig. 2. For all graphs, n=4 or 5 for WT and *Lmo3*$^{-/-}$ for rostral and caudal levels and n=3 for WT and 4 for *Lmo3*$^{-/-}$ for the middle level).

[Graphs indicate mean values; error bars show SEM. Two-tailed *t* test, $*p < 0.05$, $**p < 0.01$, $***p < 0.001$] Scale bars: (**E**) 200 μm; (**H**) 50 μm. Abbreviation: Str, striatum.

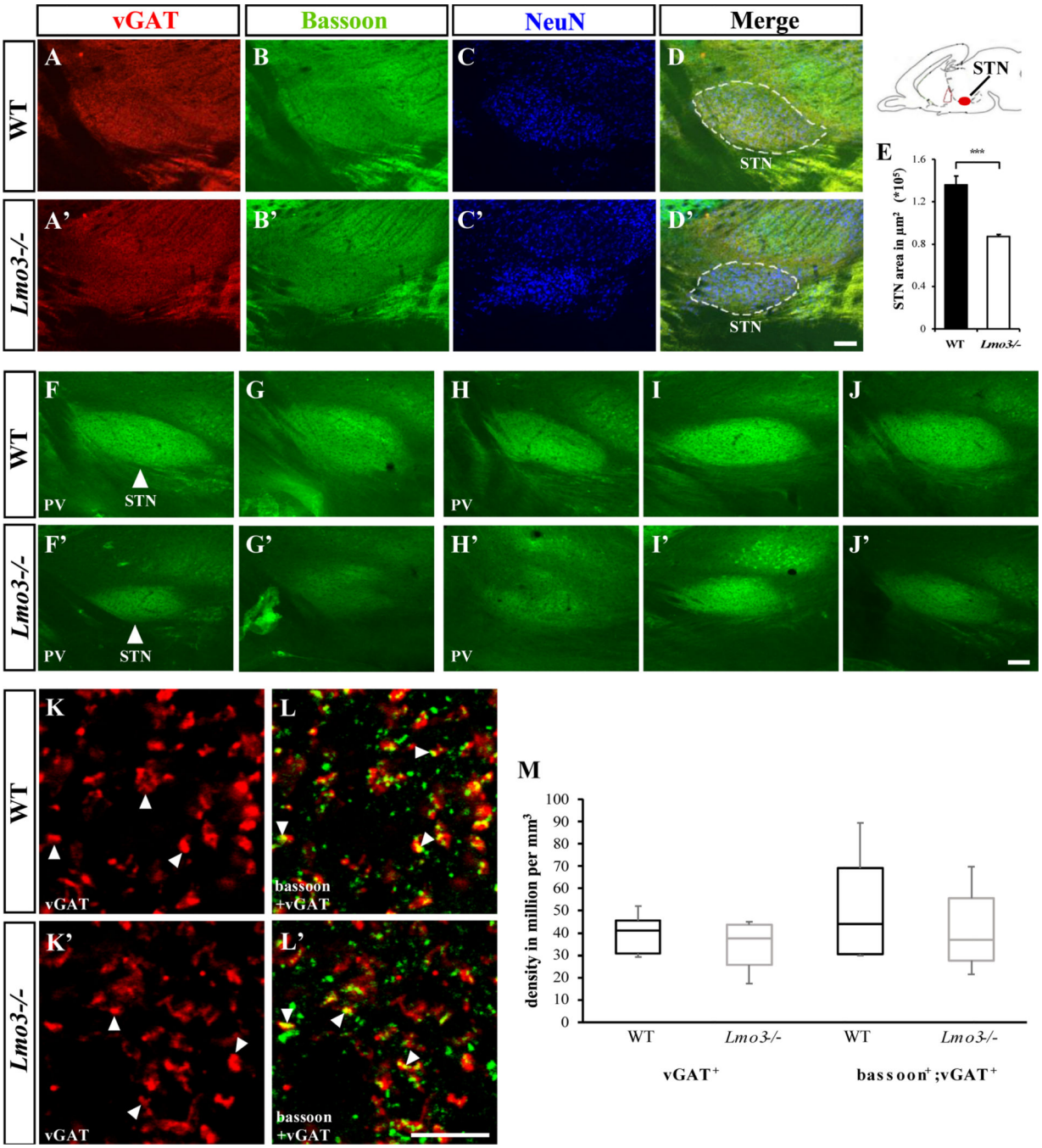

Figure 5.

Loss of Lmo3 results in a reduction of the pallidosubthalamic input. Immunostaining for the presynaptic markers vGAT (**A**,**A'**) bassoon (**B**,**B'**) and NeuN (**C**,**C'**) in sagittal sections of subthalamic nucleus (STN) at similar medio lateral levels of wildtype and *Lmo3*-null mutants. **E**, Quantification of size of inhibitory input using NeuN to demarcate the STN (dashed outlines in **D**,**D'**), reveals a significant reduction in the *Lmo3*-null mutants (**E**), n=5 for WT and *Lmo3*$^{-/-}$ [Graph indicates mean values; error bars show SEM. Two-tailed t test, p = 0.00052] **F**-**J**, **F'**-**J'** show STN stained with PV antibody. **F**,**G** and **F'**,**G'** are

sections from one mouse each for WT and *Lmo3−/−* and **H**-**J**, **H'**-**J'**, are from a second mouse. Arrowheads indicate the STN, which is smaller in size in the *Lmo3*-null mutants. **K**,**K'**, are representative confocal micrographs of vGAT immunostaining in the STN of WT and *Lmo3−/−* mice, respectively; **L**,**L'** demonstrate bassoon double immunostaining. Filled arrowheads indicate examples of $vGAT^+$ and $bassoon^+;vGAT^+$ structures counted. **M**, Box-and-whisker plots showing density of $vGAT^+$ (left) and $bassoon^+;vGAT^+$ structures (right) in the STN of WT and *Lmo3−/−* mice. Boxes denote first, second (median) and third quartiles, while whiskers represent the 10^{th} and 90^{th} percentiles. n=8 for WT and Lmo3−/− for quantification of $vGAT^+$ and n=7 for quantification of $bassoon^+;vGAT^+$ structures. [Mann-Whitney U test, $p = 0.193$ for $vGAT^+$ and $p = 0.5221$ for $bassoon^+;vGAT^+$] Scale bars: (**D'**,**J'**) 100 μm; (**L'**) 5 μm.

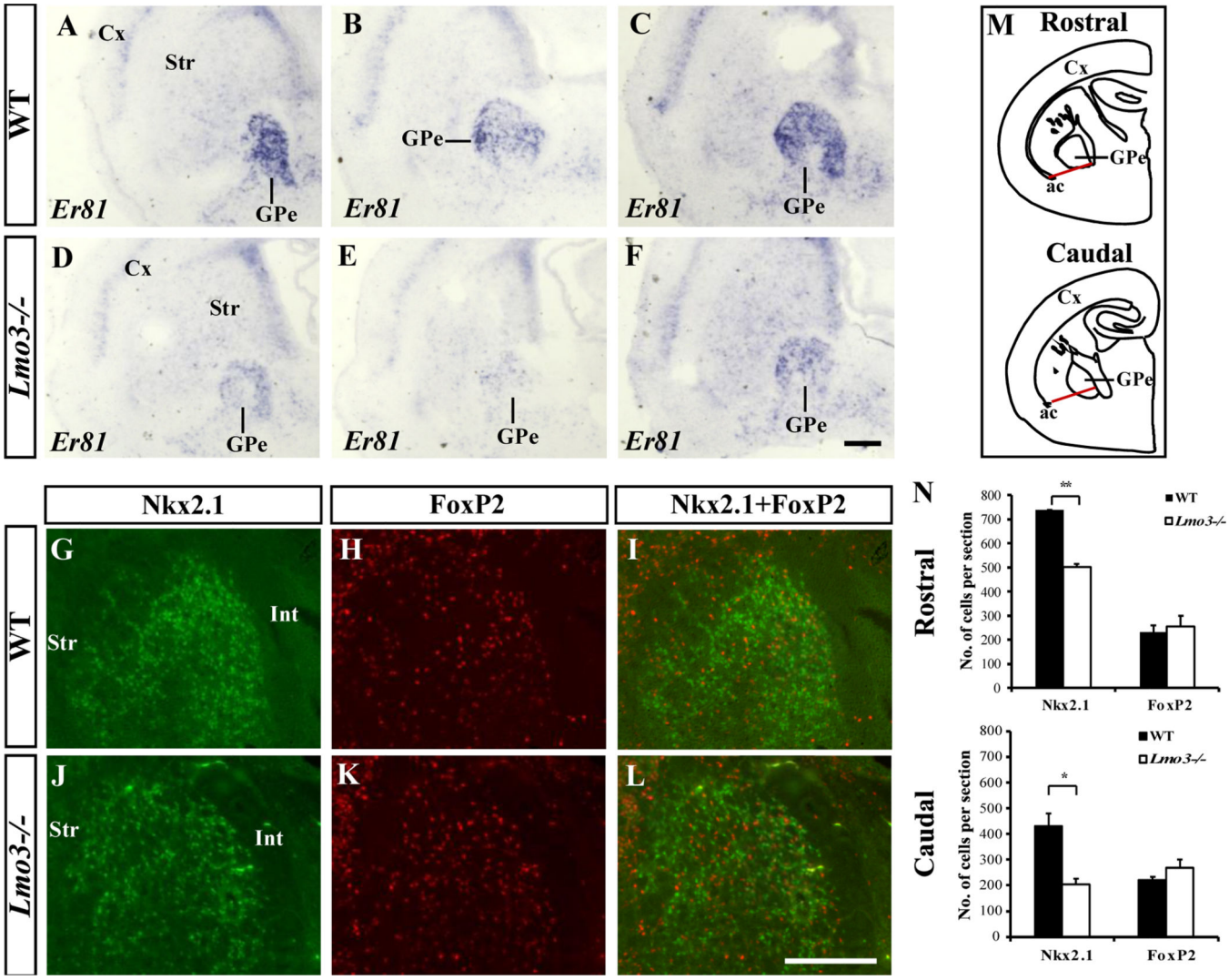

Figure 6.

Reduction of MGE derived GPe neurons in the *Lmo3*-null mutant at P0. **A**-**F**, *in situ* RNA hybridization staining at three different rostrocaudal levels shows strong *Er81* expression labeling the P0 GPe in WT (**A**-**C**), and a marked reduction in the *Lmo3*−/− GPe (**D**-**F**). **G**-**L**, Immunohistochemistry for Nkx2.1 and FoxP2 in the GPe of wildtype (**G**-**I**) and *Lmo3*-null **J**-**L**) mutants. **M**, Coronal sections illustrating 2 different rostrocaudal levels of the GPe from which neurons were counted. Ventral borders of the GPe (red lines) were defined according to the medial edge of the anterior commissure (ac). **N**, Quantification shows a significant reduction of $Nkx2.1^{+}$ neurons in the *Lmo3*−/− GPe at both rostrocaudal levels. No significant differences in $FoxP2^{+}$ neuron numbers were observed between *Lmo3*−/− and WT ($n = 3$ each for WT and *Lmo3*−/− for both graphs). [Graphs indicate mean values; error bars show SEM. Two-tailed t test, for rostral level $p = 0.003$ for Nkx2.1 and 0.709 for FoxP2; for caudal level $p = 0.035$ for Nkx2.1 and 0.324 for FoxP2. $*p < 0.05$, $**p < 0.01$]. Abbreviations: Cx, cortex; GPe, external globus pallidus; Int, internal capsule; Str, striatum. Scale bars: 200 μm.

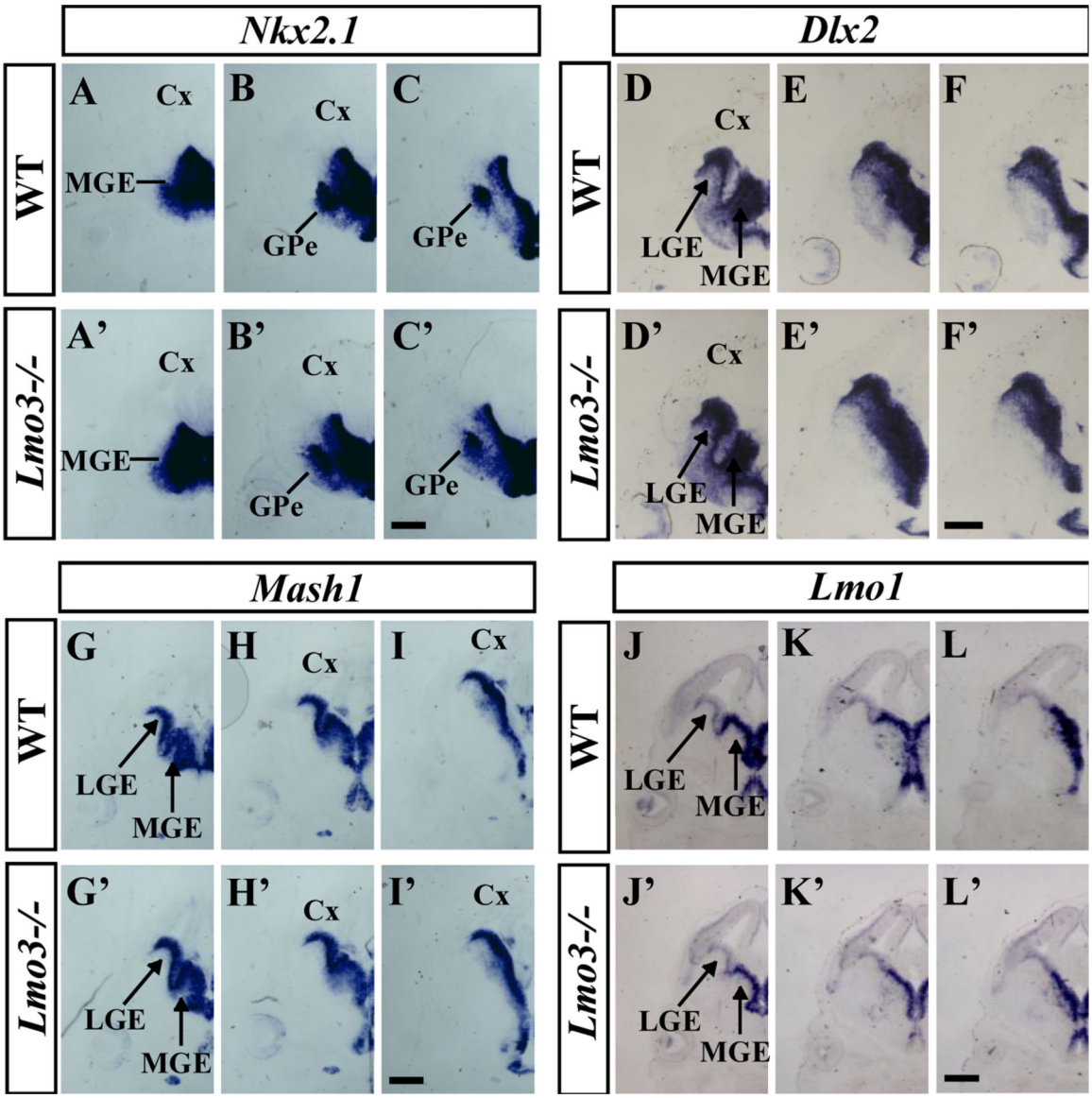

Figure 7.

Expression of subpallial markers in the control and *Lmo3*-null mutant at E13.5. Images of three serial coronal hemisections (rostral-most on the left) show *in situ* RNA hybridization staining at E13.5 for *Nkx2.1* (**A-C**, **A'-C'**), *Dlx2* (**D-F, D'-F'**), *Mash1* (**G-I, G'-I'**) and *Lmo1* (**J-L, J'-L'**). Abbreviations: Cx, cortex; GPe, external globus pallidus; LGE, lateral ganglionic eminence; MGE, medial ganglionic eminence. Scale bars: 500 μm.

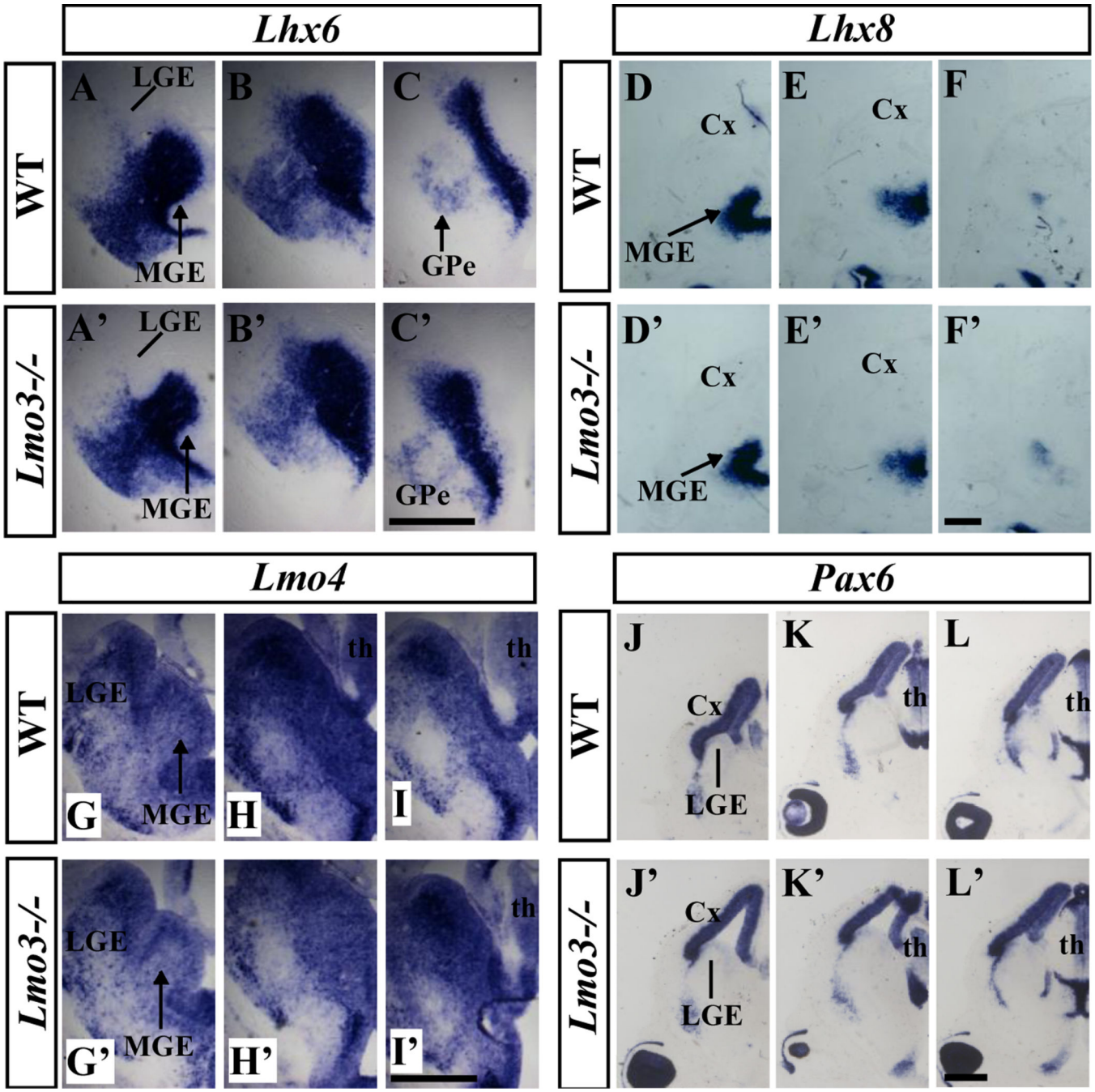

Figure 8.

Expression of MGE and LGE markers is unchanged in the *Lmo3*-null mutant at E13.5. Images of three serial coronal hemisections (rostral-most on the left) show *in situ* RNA hybridization staining for *Lhx6* (**A-C**, **A'-C'**), *Lhx8* (**D-F**, **D'-F'**), *Lmo4* (**G-I**, **G'-I'**) and *Pax6* (**J-L**, **J'-L'**). Abbreviations: Cx, cortex; GPe, external globus pallidus; LGE, lateral ganglionic eminence; MGE, medial ganglionic eminence; th, thalamus. Scale bars: 500 μm.

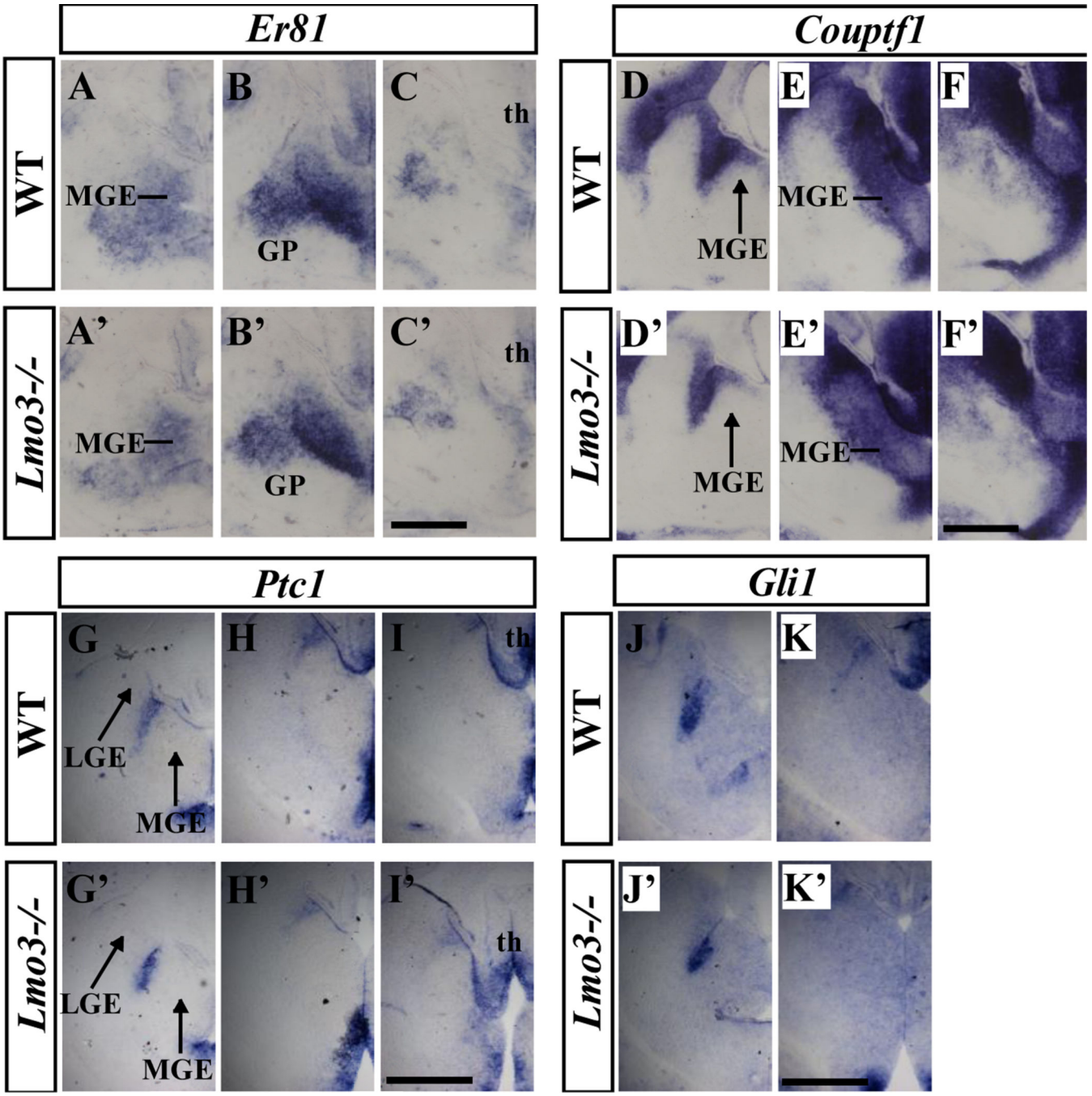

Figure 9.

Expression of selected MGE markers is unchanged in the *Lmo3*-null mutant at E13.5. Images of three serial coronal hemisections (rostral-most on the left) show *in situ* RNA hybridization staining for *Er81* (**A-C**, **A'-C'**), *Couptf1* (**D-F**, **D'-F'**), *Ptc1* (**G-I**, **G'-I'**) and *Gli1* (**J**,**K**,**J'**,**K'**). Cx, cortex; GPe, external globus pallidus; LGE, lateral ganglionic eminence; MGE, medial ganglionic eminence; th, thalamus. Scale bars: 500 μm.

Table 1

Neuronal makeup of the GPe

	PV$^+$			**FuxP2$^+$**			**Nkx2.1$^+$**			**Npas1$^+$**	
	% of total GPe neurons	***n* (mice)**	**WT vs *Lmo3*−/− *p* value**	**% of total GPe neurons**	***n* (mice)**	**WT vs *Lmo3*−/− *p* value**	**% of total GPe neurons**	***n* (mire)**	**WT vs *Lmo3*−/− *p* value**	**% of total GPe neurons**	***n* (mice)**
WT	45.9 ± 3.7	4	0.02	24 ± 1	3	0.01	64.7 ± 1.5	3	0.001	34.8 ± 0.8	2
Lmo3−/−	30.4 ± 1.6	3		40 ± 3.3	4		49.4 ± 1.2	3		46.2 ± 0.4	2

% values indicate mean ± SEM; *p* values are from two-tailed *t* tests.

NeuN was used as the marker for total GPe neuron counts per section.

For each *n* of all 4 molecular markers, counts were obtained from 2–3 sections per level (Fig. 2I).